UvA-DARE (Digital Academic Repository)

An empirical isochrone of very massive stars in R136a

de Koter, A.; Heap, S.R.; Hubeny, I.

AN EMPIRICAL ISOCHRONE OF VERY MASSIVE STARS IN R136a[1]

ALEX DE KOTER,[2,3] SARA R. HEAP,[4] AND IVAN HUBENY[4,5]

ABSTRACT

We report on a detailed spectroscopic study of 12 very massive and luminous stars ($M \gtrsim 35 M_\odot$) in the core of the compact cluster R136a, near the center of the 30 Doradus complex. The three brightest stars of the cluster, R136a1, R136a2, and R136a3, have been investigated earlier by de Koter, Heap, & Hubeny. Low-resolution spectra (< 200 km s^{-1}) of the program stars were obtained with the GHRS and FOS spectrographs on the Hubble Space Telescope. These instruments covered the spectral range from 1200 to 1750 Å and from 3200 to 6700 Å, respectively. Fundamental stellar parameters were obtained by fitting the observations by model spectra calculated with the unified ISA-WIND code of de Koter et al. supplemented by synthetic data calculated using the program TLUSTY. We find that the stars are almost exclusively of spectral type O3. They occupy only a relatively narrow range in effective temperatures between 40 and 46 kK. The reason for these similar $T_{\rm eff}$'s is that the isochrone of these very massive stars, which we determined to be at ~2 Myr, runs almost vertically in the H-R diagram. We present a quantitative method of determining the effective temperature of O3-type stars based on the strength of the O v $\lambda1371$ line. Present-day evolutionary calculations by Meynet et al. imply that the program stars have initial masses in the range of $M_i \sim 37$–76 $M_\odot$. The observed mass-loss rates are up to 3 (2) times higher than is assumed in these evolution tracks when adopting a metallicity $Z = 0.004$ (0.008) for the LMC. The high observed mass-loss rates imply that already at an age of ~2 Myr the most luminous of our program stars will have lost a significant fraction of their respective initial masses. For the least luminous stars investigated in this paper, the observed mass loss agrees with the prediction by the theory of radiation-driven winds (Kudritzki et al.). However, for increasing luminosity the observed mass loss becomes larger, reaching up to 3–4 times what is expected from the theory. Such an increasing discrepancy fits in with the results of de Koter et al., where an observed overpredicted mass-loss ratio of up to 8 was reported for the brightest members of the R136a cluster, for which $M_i \sim 100$ $M_\odot$ was found. The failure of the theory is also present when one compares observed over predicted wind momentum as a function of wind performance number. This strongly indicates that the shortcoming of the present state of the theory is connected to the neglect of effects of multiple photon momentum transfer.

Subject headings: Magellanic Clouds — stars: early-type — stars: evolution — stars: fundamental parameters — stars: mass loss — ultraviolet: stars

1. INTRODUCTION

This paper is part of a series in which we will study the properties of individual stars in Radcliffe 136a, the central cluster of the 30 Doradus H II region in the Large Magellanic Cloud (LMC). R136a contains a very dense population of young, massive stars. In previous papers, we have discussed observations and theoretical modeling of a number of the brightest members of R136a, namely R136a1, R136a2, R136a3, and R136a5 (Heap et al. 1994; de Koter et al. 1994; de Koter, Heap, & Hubeny 1997, hereafter KHH). These stars show hybrid Wolf-Rayet–like and O-type–like spectra. In this paper, we will derive photospheric and wind parameters of 12 very luminous early O-type stars in the center of the cluster, using ultraviolet and optical spectra obtained with the Goddard High Resolution Spectrograph

(GHRS) and Faint Object Spectrograph (FOS) on board the Hubble Space Telescope (HST). The observational methods used to secure these spectra are so complex that they warrant a separate paper (Heap et al. 1998). The modeling methods employed in this study use the most recent versions of the ISA-WIND code of de Koter, Schmutz, & Lamers (1993) and the TLUSTY program of Hubeny & Lanz (1995).

In 1983, Savage et al. studied ultraviolet spectra of R136a taken with the International Ultraviolet Explorer satellite. They concluded that either R136a is a compact cluster of normal stars containing about 30 very early O and WN stars or that the light of the object is dominated by the presence of one or a few supermassive stars. Because the first option requires the presence of tens of the rarest stars found in Galactic systems within a single stellar cluster, they opted for the supermassive star scenario. Not much later, however, Melnick (1985) showed that this scenario could not be the right one as he observed that with ever-increasing instrumental resolution, more and more individual stars could be resolved near the "edge" of R136a. After the first servicing of the HST in 1993 December, it became possible for the first time to resolve individual stars in the very center of the cluster.

It was expected that the three brightest members would be highly evolved Wolf-Rayet stars as this was indicated by

[2] Advanced Computer Concepts, Code 681, Goddard Space Flight Center, Greenbelt, MD 20771.
[3] Astronomical Institute "Anton Pannekoek," University of Amsterdam, Kruislaan 403, NL-1098 SJ, Amsterdam, Netherlands; dekoter@astro.uva.nl.
[4] Laboratory for Astronomy and Solar Physics. Code 681, Goddard Space Flight Center, Greenbelt, MD 20771; hrsheap@hrs.dnet.nasa.gov.
[5] AURA, National Optical Astronomy Observatories, Code 681, Goddard Space Flight Center, Greenbelt, MD 20771; hubeny@stars.gsfc.nasa.gov.

the strength of the He II λ4686 emission line (Campbell et al. 1992; Parker, Heap, & Malumuth 1995). However, it was found by KHH that these stars are rich in hydrogen and that they are in fact young main-sequence, hydrogen-burning stars, albeit stars featuring a mass loss so large that it is typical for real Wolf-Rayet stars. Such an unexpected mass-loss behavior has important implications for our understanding of very massive star evolution, as it is predominantly mass loss that "drives" the stars through subsequent phases of Of-type, luminous blue variable, and Wolf-Rayet stars.

The above summary of developments raises many questions that need to be addressed. They include the following: Why is R136a so extremely rich in stars of the earliest defined spectral type O3? Are the mass-loss rates of these O3-type stars also much higher compared to Galactic counterparts, as has been found for the very brightest cluster members? If so, (1) do they also experience a main-sequence hydrogen-rich WNL-phase? (2) Can their mass-loss rates still be explained in the context of the theory of radiation-driven winds—which predicts a lower mass loss for stars in a lower metallicity environment such as the LMC—or play other effects, such as rotation or (pulsational) instabilities, a role in the wind-driving mechanism of very massive stars in the early main-sequence phase? (3) What does the mass loss versus metallicity dependence look like based on R136a and Galactic stars? Or, encompassing all these questions in a more general one: if the mass-loss rates are different, how do very massive stars evolve? To illustrate briefly the comprehensive nature of this last question, one may for instance wonder about such wide-ranging problems as (a) do the most massive stars shed so much mass that they reduce their final mass to below the limit of black hole formation? (b) If the main-sequence early O and Wolf-Rayet–like stars provide substantial He II emission, how does this affect the interpretation of the star formation history in distant starbursting clusters and galaxies?[6]

In this paper, we will attempt to answer some of the questions posed above. Our main focus will be to derive an empirical isochrone for very massive stars, which would obviously provide an important calibrator for scenarios of very massive star evolution. For such a venture, the R136a cluster is ideal as (1) its distance is well known, (2) it is rich in very massive stars, and (3) its compact size implies coeval star formation. For this isochrone to prove meaningful as a reference for a new generation of evolution track calculations, we also need to derive reliable mass-loss rates. This will be the second main focus of this study.

In § 2 we will briefly discuss the observations. As mentioned above, the observation technique is so intricate that it needs a separate publication for which we refer to Heap et al. (1998). The modeling approach is treated in § 3, where we will point out that for our problem an accurate determination of especially effective temperature, T_{eff}, and mass loss, $\dot{M}$, is of crucial importance. Our T_{eff}-calibration will be based on the strength of the O V λ1371 line. This method may not be ideal, but it is the best available as in this particular case the classical approach fails because of the limited resolution and signal-to-noise ratio (S/N) of the FOS spectra. Our $\dot{M}$ calibration will be based on the strength of the stellar wind emission in Hα. Our consistent treatment of this diagnostic represents the most accurate method of determining the mass loss of our program stars. The results will be presented in § 4. In § 5, we will compare our derived mass-loss rates with results of other analyses of luminous and massive stars, especially those results frequently used in evolutionary track calculations. The subsequent section compares our mass loss findings with predictions by radiation-driven wind theory. Finally, in § 7, we briefly summarize the most important results of this study and present the empirical isochrone of very massive stars in R136a.

2. OBSERVATIONS AND REDUCTIONS

In contrast to spectroscopic surveys that are being carried out on R136, our program is directed toward establishing the fundamental properties of a young cluster with massive stars, thereby generating an empirical isochrone for young, massive stars. To ensure that the stars are coeval, we selected as program stars only those stars at the very core of R136—stars within the dense cluster known as R136a. The maximum range in ages among the program stars is ∼100,000 yr, estimated as the sound-travel time through the cluster. To determine the fundamental properties of a star including mass-loss parameters requires both the GHRS and FOS spectra, which form a complete data set sufficient for quantitative analysis. As will be described in § 3, the GHRS ultraviolet spectra provide information about spectral type, effective temperature, and the structure of the wind; the FOS spectra, information on spectral type, extinction, and mass-loss rate.

The observing program and results are described in detail by Heap et al. (1998). Here we give only a brief summary of the observations. The observing program (HST program 6018), covering 34 spacecraft orbits in the continuous viewing zone, was carried out in 1996 February. Table 1 lists the program stars. They include 16 stars in R136a and R136b, which lies 2″ from the core of R136a. The second and third columns give the star identification and visual magnitude, respectively (from Malumuth & Heap 1994). The FOS was used to observe all 16 stars in the G400H and

[6] In the field of starbursts, one typically assumes that the He II emission originates from evolved Wolf-Rayet stars. Overestimated W-R/O-star ratios would—erroneously—favor short-burst scenarios.

TABLE 1
Observed Parameters of the Program Stars

	Name	V (mag)	v_{edge} (km s^{-1})	W_{obs} (Å)	
				O V	Hα
	637 B	13.17	2069	−3.48	−18.65
	498 A1	12.77	3624	−3.65	−48.15
	467 A3	12.93	3369	−3.41	−71.13
	511 A2	13.38	3446	−3.37	−47.59
1	519 A5	13.73	3523	−4.22	−17.18
2	509 A7	13.73	3398	−3.56	−0.75
3	618	14.25	3955	−4.58	−3.98
4	608	14.39	4287	−5.41	−14.24
5	535	14.49	3473	−4.46	0.07
6	354	14.52	3346	−3.12	0.90
7	553	14.56	3514	−3.56	1.45
8	508	14.51	3419	−2.96	1.90
9	602	14.63	4039	−4.49	−1.05
10	551	14.81	3715	−4.18	1.61
11	533	14.81	3572	−2.85	0.16
12	542	14.86	3599	−3.72	−1.44

Note.—Star R136a-354 is a spectroscopic binary.

G570H grating modes, producing spectra covering the spectral range from 3200 Å to 6700 Å at a spectral resolution of 2.5–5.0 Å. The exposure time was adjusted such that in all cases a signal-to-noise ratio of at least 80 per resolution element (detector diode) was achieved. The GHRS was used in its low-resolution mode, G140L, to obtain spectra spanning 1150–1750 Å at a resolution of 0.5 Å. Only those 12 stars that had not previously been observed by GHRS were observed in this program. The GHRS observations and analysis of the other four stars are described in references: Heap et al. (1994) and de Koter et al. (1994) for R136a5; de Koter et al. (1997) for R136a1, R136a2, and R136a3.

The size of the FOS B-3 aperture is 0″.28. Because of the small spatial separation of the cluster members, one runs the risk of contaminating spectra with light from nearby stars. This is indeed a valid concern for stars R136a-618 and R136a-553, which are separated by only $\sim$0″.1 from stars R136a-621 and R136a-538, respectively. We tried to avoid this problem by offsetting the aperture slightly, with satisfactory results. In general the crowding problem appeared to be manageable. We believe that for none of the 12 program stars significant contamination has occurred (see Heap et al. 1998 for details). Star R136a-354 is identified as a spectroscopic binary, having spectral type O3 V + O3–4 V according to Heap et al. (1998) and O3 V + O3–5 V following Massey & Hunter (1998). We have not included this system in the derivation of mass-loss parameterizations (see § 5). The presence of a diffuse nebular emission may influence the optical lines. Especially, emission of the ionized gas in hydrogen and nitrogen may contribute to the Hα profile—which is our main mass-loss diagnostic. At the size of the FOS aperture, the nebular emission at Hα has a width of 3.7 Å (somewhat less than the FOS resolution of 5.0 Å). The relatively weak stellar Hα profiles turn out to be only slightly broader, which makes it difficult to detect the presence of nebular emission. If nebular emission is present, it may lead to an overestimate of the mass loss for the relatively low luminosity, consequently relatively low mass loss stars in our sample.

3. SPECTROSCOPIC ANALYSIS

In this section, we will discuss the approach to our spectroscopic analysis. The presented models are calculated using the most recent versions of the non-LTE unified[7] improved Sobolev approximation code ISA-WIND for stars with stellar winds (de Koter et al. 1993; KHH) and the plane-parallel non-LTE model atmosphere code TLUSTY (Hubeny & Lanz 1995). Here, we will not discuss model assumptions or numerical methods, which are treated in detail in the above-mentioned references, but suffice it to say that for the ISA-WIND models the atmospheric structure and chemical composition is similar to that used in KHH.

Our initial idea was to derive photospheric parameters (T_{eff}, log g) from TLUSTY calculations and to obtain the wind properties [$\dot{M}$, $v(r)$] from ISA-WIND models. However, the quality of the spectra and the high effective temperatures and mass-loss rates of the program stars cause the standard diagnostic method of constructing so-called

---

[7] We use the word "unified" to indicate that no artificial separation between photosphere and wind is assumed.

T_{eff}–log g fit diagrams based on plane-parallel models to fail. In the fit-diagram method, one essentially uses optical H and He lines to try to find the best log g value for a set of T_{eff} values for given v sin i and H/He abundance ratio (Kudritzki 1980). The main reason that this method fails is that the resolution of the FOS (2.5–5.0 Å) is too coarse and the S/N ($\sim$80) somewhat too modest for detailed profile analysis. An extra complication is that all program stars are hotter than $\sim$40 kK, which implies that He i lines are either absent or very weak. This prohibits the use of the He i to He ii ratio as a temperature indicator. Also, the "photospheric" profiles of H i, He i, and He ii lines may be partly filled in by nebular emission and by emission from the extended wind.

This implies that one needs to resort to the use of unified non-LTE models for both the determination of photospheric and wind parameters. Unfortunately, this is a formidable task because of the computer-intensive nature of calculating such models for a large number of stars. Still, we have opted to travel this road in order to present results for a relatively large number of stars using a consistent modeling technique. Our approach implies that we needed to limit the exploration of certain shortcomings in the current state of our models. This opposed to the philosophy of, in particular, Pauldrach et al. (1994, hereafter PKPBH), in which the deficiencies of the models are analyzed in great depth for only a few stars. In our setup we tried to select a few key spectroscopic features from which to derive (at least first estimates of) all stellar parameters. Such a strategy requires knowledge of the sensitivity of spectral lines to different stellar parameters. So, in the next sections, where we will outline our method, we will start out by calculating a grid of unified O-type star models covering the anticipated parameter space. This grid will be used to derive quantitative diagnostics for the determination of the most critical parameters, i.e., temperature and mass loss. The temperature diagnostic will be based on the strength of the O v λ1371 line, which is primarily sensitive to T_{eff}. The mass-loss diagnostic will be based on the observed strength of Hα corrected for "photospheric" absorption.

3.1. The Grid of ISA-WIND Models

The grid of ISA-WIND models—to be used *only* to set up the temperature and mass-loss diagnostics—is based on the *Galactic* O-type star spectral classification of Howarth & Prinja (1989). The grid contains models for eleven different spectral types (O3, O4, O5, and O6–O9.5 in steps of one-half a spectral type) and five luminosity classes. H-R diagram positions and stellar masses for luminosity class II and IV are interpolated in log ($L/L_{\odot}$) and log T_{eff} from classes I, III, and V. Mass-loss rates are assigned using the fitting formula derived by Lamers & Leitherer (1993). Values for v_{∞} follow from the proportionality relation between effective surface escape velocity and terminal flow velocity, given by Lamers, Snow, & Lindholm (1995). The supersonic wind velocity structure is given by a β-law, where $\beta = 1$. The chemical elements included in the grid calculation are H, He, C, N, O, and Si.

As we will point out in §§ 3.3 and 3.6, the actual values of the adopted grid parameters are not of crucial importance for constructing the T_{eff} and $\dot{M}$ diagnostics. Note that the mass-loss formula of Lamers & Leitherer is for a Galactic metallicity. So, the $\dot{M}$ values in the grid are about twice that expected for LMC stars (assuming $Z = \frac{1}{4} Z_{\odot}$ and a
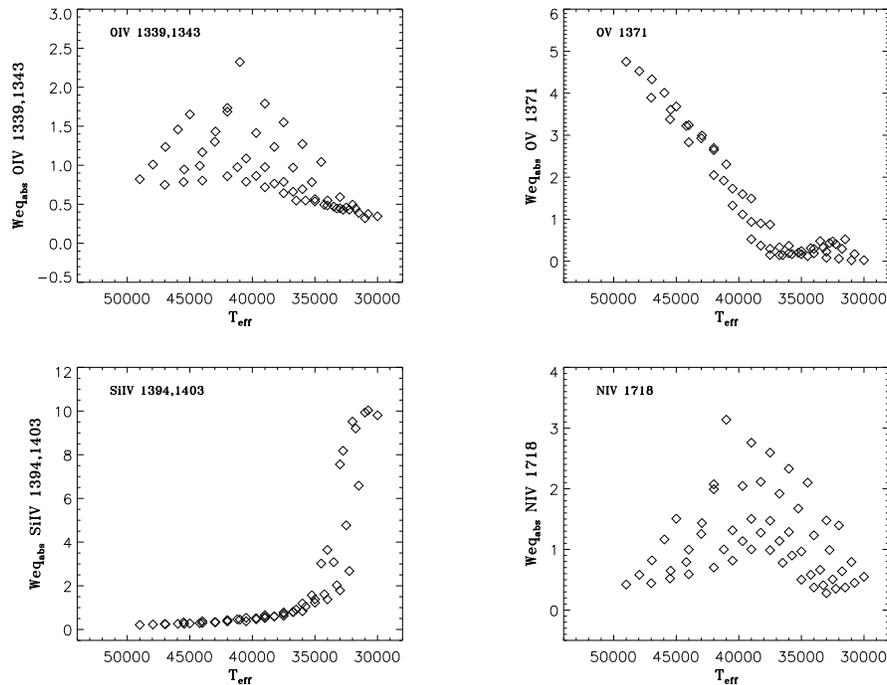
FIG. 1.—Absorption equivalent width of all the $1\dot{M}_{Gal}$ grid models. One clearly sees that O IV $\lambda\lambda1338$, 1343 and N IV $\lambda1718$ are sensitive to both mass loss and temperature. This also holds for Si IV $\lambda\lambda1394$, 1403; however, for our purposes this line is of only limited use, as it is not observed as a wind line in the hot R136a stars. The O V $\lambda1371$ line shows an almost linear increase in strength with temperature, which makes it a useful T_{eff} diagnostic.

mass-loss metallicity dependence $\dot{M} \propto Z^{1/2}$). However, it is advantageous to adopt a relatively high mass loss as several of the program stars show Of or even Of/WN-type features in their spectra. The most luminous stars even required the calculation of a grid in which the *Galactic* mass loss has been multiplied by a factor of 2. Where necessary, these two grids of models will be referred to as the $1\dot{M}_{Gal}$ and $2\dot{M}_{Gal}$ grid.

3.2. *The Modeling Strategy*

In short, our modeling strategy will be as follows: (1) In the first step, we will use the O V $\lambda1371$ line to derive the effective temperature. (2) Using a $BC(T_{eff})$ relation, and a first estimate for the extinction, we derive luminosities and stellar radii. (3) We determine the terminal flow velocity from the C IV $\lambda\lambda1548$, 1550 resonance line. (4) Next, we derive the mass-loss rate using the strength of the observed Hα line corrected for its "photospheric" absorption. (5) Using the resulting parameters, we calculate an ISA-WIND model for each star. This model is then used to rederive the extinction, yielding improved values of the absolute magnitude and other related quantities (i.e., radius and mass loss). (6) In the final step, we tune the parameters as derived in the first five steps by calculating unified non-LTE models and comparing these with the observations.

In the remainder of this section, we will discuss the first five steps in detail. The final set of parameters and the quality of the spectral fits will be discussed in the next section.

3.3. *Effective Temperature*

Because we cannot use the optical H and He lines for the temperature determination (see above), we need to resort to using lines in the ultraviolet part of the spectrum. Several of the distinct features in the GHRS spectrum (covering the

wavelength range from 1200 to 1750 Å) immediately disqualify as a possible temperature diagnostic. These include the mostly saturated N V $\lambda\lambda1238$, 1242 and C IV $\lambda\lambda1548$, 1550 resonance doublets as well as the He II $\lambda1640$ line, which in the range of interest (i.e., $T_{eff} \sim 40$–50 kK) is mostly insensitive to temperature (de Koter et al. 1994; KHH). Apparent candidates, on the other hand, are the O IV $\lambda\lambda1338$, 1343 and O V $\lambda1371$ lines and N IV $\lambda1718$. Finally, the Si IV $\lambda\lambda1394$, 1403 doublet, although not observed, may serve as a lower limit indicator.

Figure 1 shows the equivalent width of absorption of these last four lines as a function of temperature, for all models in the O-star grid. This equivalent width is defined as the integral over the absorption part of the profile only. The adopted metallicity is $Z = \frac{1}{4} Z_{\odot}$, following the work of PKPBH for the O3 If/WN–type star Melnick 42 located some 8″ outside the core of R136a (Walborn et al. 1992). The O IV and N IV lines clearly show a dependence on both T_{eff} and $\dot{M}$. The absorption in both lines is strongest for the
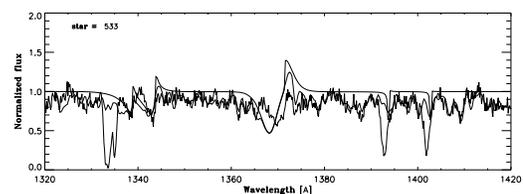

FIG. 2.—Observed and (representative) theoretical spectra of star R136a-533. We have overplotted (1) a theoretical spectrum containing only the potential wind lines of O IV, O V, and Si IV (*thin line*) and (2) a fully line blended synthetic spectrum (*thick line*). The latter fit is excellent and even allows for an accurate determination of the system velocity. The line-blended spectrum is used to properly account for the metal blends of the O V line.
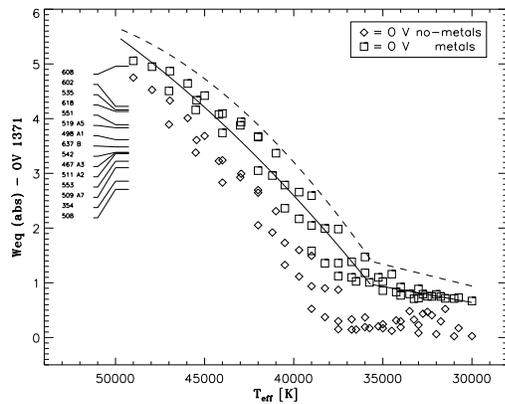
Fig. 3.—Total absorption equivalent width in the wavelength range from 1360 to 1372 Å, in which is located the blueshifted absorption of O v, vs. effective temperature. The diamonds refer to calculations without line blending; the squares are for those in which the blending by thousands of metal lines is included. The inclusion of blending leads to a shift of the temperature scale by ~ -2500 K. The solid line gives the best fit for the adopted metallicity $Z = \frac{1}{4} Z_\odot$. For comparison, the dashed line gives the best fit if one would assume $Z = \frac{1}{2} Z_\odot$.

O5 I model, which has the largest mass loss in the grid (log $\dot{M} = -4.99$). The lower left-hand panel in Figure 1 shows that above ~ 37 kK, the Si IV line is a photospheric absorption line. For temperatures down to ~ 30 kK, the line is very sensitive to mass loss. Because of this reason and because of the mass loss versus luminosity relation for early-type stars, this line is a good luminosity diagnostic for mid O-type stars. Clearly, the absence of any significant Si IV wind emission in our program stars implies that all stars are hotter than 37 kK.

The O v line shows an altogether different behavior. This line is no longer present in significant strength at $T_{\text{eff}} \lesssim 37$ kK. For higher temperatures, however, it shows an almost linear increase in strength with temperature. Moreover, the relation is fairly tight, which indicates that the line is mostly sensitive to temperature and relatively insensitive to, *but not independent of,* mass loss. A strong O v wind profile and essentially no Si IV is a unique feature of O3 giants and supergiants (Walborn, Nichols-Bohlin, & Panek 1985; Walborn & Nichols-Bohlin 1987; Walborn et al. 1995). Following this criterion, we classify all our program stars as of spectral type O3. This is consistent with the analysis of Massey & Hunter (1998) who investigated a sample of 65 of the bluest, most luminous stars in R136. They found that— not counting the W-R–like stars R136a1, R136a2, and R136a3—39 of these have the earliest defined spectral type. Nine of the 12 stars in our sample are included in their study. All of these are classified as O3, except for star R136a-508 (number 39 in their identification scheme), which is awarded spectral class O4V((f)) plus a possible contribution from an O6 star. For star R136a-508, we derive $T_{\text{eff}} = 40.6$ kK, which is the lowest value in this subset of nine stars.

We will use the absorption equivalent width of O v as our quantitative temperature diagnostic. We believe that this approach will at least result in a reliable *relative* temperature scale, provided all stars have the same surface oxygen abundance. We will return to this last point in § 4, where we will show that this assumption is indeed valid for all our program stars except for R136a5. We cannot easily exclude that our temperature calibration may be subject to

a systematic shift. Several effects may cause such a shift: (1) contamination of the oxygen line profile by the many metal lines present in the spectral range around 1371 Å; (2) the adopted LMC metallicity; (3) the choice of the observed continuum in the region of the O v line; (4) errors in the O v ionization and excitation balance due to, most notably, the neglect of a consistent treatment of metal line blanketing in our models. We will discuss all these effects in the given order.

The contamination by metal lines is illustrated in Figure 2. The observed spectrum of star R136a-533 is plotted together with a representative fit. Although the present discussion is concerned with the blending by metal lines, the fit shows that too much emission is predicted for O v and that the absorption is too much shifted toward the blue. We will return to this below. Comparing the blue wing of the theoretical profile with the observed spectrum shows that, if no attempt is made to correct for the presence of metal lines, the measured equivalent width may be overestimated as it is difficult to determine which part of the observed absorption is due to O v and which part is due to metal blends. An overestimated equivalent width would result in an overestimate of the effective temperature.

In order to assess the importance of this problem—and to correct for it—we have also modeled the blending by metal lines using a generalized form of the modified nebular approximation (Schmutz 1991) to describe the ionization/excitation equilibrium of those metals not explicitly treated in ISA-WIND. This method is described in detail in KHH, where it is used to perform Monte Carlo simulations with the intent of studying the wind driving mechanism. The essential difference in the way it is applied here, is that we have used the modified nebular approximation in the formal solution to obtain the synthetic spectrum. A second difference is that for this work, we have used the Kurucz line list (Kurucz 1988).

The resulting metal line blended spectrum is given in Figure 2 (*thick line*). For comparison, we also give the non-convolved theoretical spectrum in which only O IV $\lambda\lambda 1338$, 1343, O v $\lambda 1371$, and Si IV $\lambda\lambda 1394$, 1403 have been modeled (*thin line*). The instrument profile is taken to be a Gaussian profile of width 0.57 Å.

The fit to the observed spectrum is excellent. This confirms that the modified nebular approximation provides a reliable approach, contrary to the assumption of LTE for which test calculations show that it yields flagrantly unrealistic results. The detailed fit also indicates that, in the wavelength range between 1320 and 1420 Å, the line list is apparently complete. Note that the presence of metal lines can partly explain the excess emission seen in the non-blended theoretical spectrum.

Figure 2 reveals that because of the presence of many metal lines, the absorption equivalent width of O v $\lambda 1371$ only is not a suitable diagnostics. In practice, we need to measure the absorption equivalent width in a wavelength interval comprising the blueshifted O v absorption. We opted to take an interval equal for all program stars. In order to properly measure the stars with the largest v_∞, we have adopted the range from 1360 to 1372 Å. The results are given in Figure 3. The theoretical equivalent widths including metal blending are denoted by squares; those predicted for the O v line only are indicated by diamonds. Comparing the two shows that not accounting for blending might have led to overestimated values of T_{eff} by typically ~ 2500 K.

The almost constant shift in the relation shows that the underlying metal line spectrum is not very temperature sensitive in the range from 30 to 50 kK. A mild temperature dependence is revealed at $\lesssim 36$ kK, where the O v line is not present or very weak.

On the basis of the above discussion, we define our quantitative temperature diagnostic as follows: $T_{\rm eff}$ is determined by requiring that the absorption equivalent width in the wavelength range from 1360 to 1372 Å, $W_{\rm eq}[1360, 1372]$, is matched by the model *that also has the correct mass loss and terminal velocity*. The best-fit curve given in Figure 3 is therefore only used to provide a starting value for $T_{\rm eff}$. However, as we have pointed out that O v is mostly sensitive to $T_{\rm eff}$, and not to $\dot{M}$ and v_∞, this first estimate will not be far from the final value. The second-order polynomial best-fit curve is given by

$$W_{\rm eq}[1360, 1372] = -20.832(\pm 0.298) + 8.193(\pm 2.685)T_{\rm eff}$$
$$- 0.585(\pm 0.324)T_{\rm eff}^2 , \quad (1)$$

where $T_{\rm eff}$ is in units of 10 kK. The relation is valid for $36 \lesssim T_{\rm eff} \lesssim 50$ kK. In deriving the above result, we have adopted an LMC metallicity $Z = \frac{1}{4} Z_\odot$. Observed values for $W_{\rm eq}[1360,1372]$ are given in the fourth column of Table 1.

The strength of the metal line spectrum is expected to be a function of metallicity. This implies that a change in Z will introduce a systematic shift in our temperature determination: a higher metallicity yields stronger lines, consequently lower $T_{\rm eff}$ values. The effect of metal contents on the UV spectra of hot stars has been investigated by Haser et al. (1998). They find that over large portions of the spectrum, a change in the abundance of the (often) saturated iron-group lines results in a mere vertical shift, as the crowding of these lines is such that nowhere at $\lambda < 1600$ Å can one uniquely define the continuum. To investigate the metallicity effect, we have also calculated a test grid for $Z = \frac{1}{2} Z_\odot$. A comparison between the two metallicities reveals that the $Z = \frac{1}{2} Z_\odot$ spectrum is shifted down by $\sim 3\%$ relative to the $Z = \frac{1}{4} Z_\odot$ case, i.e., we recover the behavior found by Haser et al. It implies that over the 12 Å interval in which we measure the absorption equivalent width, $W_{\rm eq}$ would increase by almost ~ 0.4 Å. The best-fit curve for the high-metallicity case is represented by the dashed line in Figure 3 and shows an increase in equivalent width of slightly over 0.4 Å, which indicates that the dominant effect of the metallicity change is caused by the iron-group lines and not by the O v $\lambda 1371$ line itself. From the figure one derives that an increase from $Z = \frac{1}{4}$ to $\frac{1}{2} Z_\odot$ corresponds to a temperature shift of about -1500 to -1800 K.[8] Physical implications of this shift, for instance for the determination of the age of R136a, will be discussed in § 7.1.

The last, but certainly not the least important point to be discussed are possible errors in the predicted O v ionization and excitation balance. Such errors may arise due to shortcomings in the physics treated in the model. We will comment on two such processes, (1) the neglect of the emission from shocks, yielding an extra source of ionization, and (2) the neglect of the effect of metal line blanketing, which is expected to lead to a lower ionization and which may influence the formation of the O v $\lambda 1371$ line.

Soft X-ray emission from OB-type stars is observed by space-based instruments, such as the *Einstein* (see, e.g., Chlebowski, Harnden, & Sciortion 1989) and *ROSAT* observatories (see, e.g., Kudritzki et al. 1996). The emission is believed to be evidence for the presence of vigorous flow disruptions or shocks in the winds of these stars (Lucy & White 1980; Lucy 1982), heating the wind locally to temperatures $T \gtrsim 10^6$ K. The shocks themselves are conceived to be caused by hydrodynamical instabilities, a mechanism first suggested by Lucy & Solomon (1970). Such instabilities are an intrinsic property of radiation driven winds (Owocki, Castor, & Rybicki 1988). However, hydrodynamical simulations for self-excited wind instabilities show that in the lower part of the wind, i.e., below ~ 1.5 stellar radii, radiative viscosity and line drag effects will effectively *eliminate* the instability (Owocki 1994). Because the O v $\lambda 1371$ line is formed mainly in this region, we do not expect shocks to be significant.

Before addressing the effects of line blanketing, it may be useful to define briefly the concepts of blending, blocking, and blanketing, respectively, as the use of this rather technical terminology throughout the paper may perhaps cause some confusion. By metal line blending is meant the inclusion of lines from elements not explicitly treated in the non-LTE model atmosphere in the calculation of the emergent spectrum. Our models use this method. The occupation of such metal levels are calculated in the modified nebular approximation (following Schmutz 1991; see KHH for details). Blending *does not* influence the excitation/ionization of explicitly treated ions nor does it have an effect on the temperature structure. If the model atmosphere is constructed such that an incident radiation field is specified (e.g., if the core-halo approximation is applied), one may include metal opacities in this incident field. The boundary radiation is then allowed to influence the excitation/ionization of the superposed atmosphere and wind. This is what is meant by metal line blocking. The PKPBH approach is an ingenious application of this approximation. Finally, by line blanketing is meant a consistent non-LTE treatment of all relevant metals. Like, e.g., hydrogen and helium, they are allowed to influence both the state of the gas as well as the temperature structure. Such a treatment of line blanketing has been developed for hydrostatic plane-parallel non-LTE atmospheres (Hubeny & Lanz 1995) but is still lacking for unified models.

We neglect the effects of metal line blanketing. A consistent treatment of these effects is anticipated to have two important consequences. First, it would result in a lower ionization as such calculations likely produce a lower EUV flux. Although this is what one may expect intuitively, one should have some reservations until a truly self-consistent non-LTE treatment of metal line blanketing in a unified atmosphere is developed. For instance, one may argue that part of the added EUV opacity in line-blanketed calculations is offset by additional multiple scatterings in the diffuse radiation field, which increases the mean intensity in the photosphere and lower part of the wind and thus again increases the ionization (Schaerer & Schmutz 1994). Second, metal line blanketing may decrease the mean intensity at 629.7 Å, i.e., at the wavelength of the O v resonance line. This line connects the ground state with the lower $2p$ $^1P^o$ level of O v $\lambda 1371$. A decrease in the radiation field at this wavelength will yield a lower excitation of the $2p$ $^1P^o$ level, consequently a weaker line. This effect has been dis-

---

[8] Note that this argument neglects the effect of EUV blocking on the O v resonance line. If blocking is important at 629.7 Å, it would weaken the $\lambda 1371$ line—reducing the derived temperature shift.

cussed in detail by PKPBH, where it could account for the initial discrepancy in the O v λ1371 fit for ζ Puppis if line blocking was neglected.

To try to get some sort of quantitative feel for the neglect of metal line opacities in our atmospheric models, it is useful to compare the T_{eff} for Melnick 42 as derived by PKPBH—whose models treat metal line blocking—and by KHH—whose models are very similar to those presented here and where metal line blocking/blanketing is *not* treated. The method of PKPBH yields an effective temperature $T_{eff} = 50.5$ kK, while KHH derive $T_{eff} = 44.5$ kK. In their models PKPBH assume the core-halo approximation; therefore, they are not able to investigate the diffuse field effect mentioned above. This may in part explain their relatively high temperature value. Moreover, they treat the photospheric blocking essentially in LTE. As shown by Hubeny & Lanz (1995) assuming strict LTE may likely overestimate the line opacity of the iron-peak elements, again resulting in a too high T_{eff}. PKPBH deviate from strict LTE by introducing three ad hoc radiation temperatures in the spectral range between 227 and 911 Å. As this empirical procedure does not directly affect the ionizing radiation field of O IV and O V (both at $\lambda < 227$ Å) the concern of adopting LTE line opacities remains.[9] Their procedure is, however, capable of directly influencing the radiation field of the O v resonance transition at 629.7 Å. If significant individual metal lines are present at this wavelength, the O v λ1371 line is expected to be weaker (see above), favoring a higher temperature. It needs to be added that the use of smoothed blocking factors by PKPBH, although in principle reasonable for computing photoionization rates, should be taken with care when computing line excitation rates. If no significant metal lines happen to be present at 629.7 Å, the O v resonance line does not feel any significant blocking. In this respect, models based on average blocking factors may produce quite spurious results. Finally, we note that in the PKPBH result the neglect of multiple scattering effects in the hydrodynamics may have played a role in adopting the very high temperature (see KHH).

This concludes the discussion of possible (systematic) errors in the temperature determination. First, we have

shown that we are able to correct for possible errors in T_{eff} due to the blending of the O v λ1371 line with many metal lines. Second, we have made an estimate of the effect of metallicity on our effective temperature diagnostic. We anticipate a shift of ~ -1500 K if Z is increased from $\frac{1}{4}$ to $\frac{1}{2} Z_\odot$, neglecting the effects of blocking on the O v resonance line. If blocking at 629.7 Å is important, it is expected to reduce the size of this shift. Third, we have discussed the main effects of metal line blocking on the λ1371 line by comparing the modeling approaches of PKPBH and KHH. We have pointed out that in some respects (neglect of diffuse field, LTE at $\lambda < 227$ Å, constraint posed by hydrodynamics) the PKPBH method likely overestimates the effects of blocking. Our procedure, on the other hand, likely underestimates these effects and may result in a systematically too low temperature by, say, some 6%. If, however, the truth is not somewhere in the middle, a larger systematic error may exist.

3.4. Interstellar Extinction

The visual magnitudes of all program stars are from Malumuth & Heap (1994). The values are reproduced in the fifth column of Table 2. For the distance to the LMC, we adopt $d = 51.2$ kpc (Panagia et al. 1991). The grid of models has been used to derive the bolometric correction relation [10]

$$BC(T_{eff}) = 27.236(\pm 0.022) - 6.745(\pm 0.052) \log T_{eff} . \quad (2)$$

This relation is very similar to the observational relation for O-type stars derived by Chlebowski & Garmany (1991). Using a solar bolometric magnitude, $M_{bol,\odot} = +4.75$ mag (Allen 1973), one finds

$$\log (L/L_\odot) = -1.576 - 0.4[V - R \times E(B-V)]$$
$$+ 2.698 \log T_{eff} , \quad (3)$$

where $R \equiv A_V/E(B-V)$. We adopt a standard optical extinction law (Savage & Mathis 1979) and $R = 3.1$. In deriving the interstellar extinction, our approach has been as follows: We used the ISA-WIND model for R136a5 (star R136a-519) from KHH to derive a first estimate of $E(B-V)$ for all program stars using the full optical FOS spectral range from 3200 to 6800 Å. We then proceeded to determine first values of all stellar parameters and to calculate and tune respective unified models. These models were in

---

[9] This argument may be of less importance if ionization from excited levels is an important mechanism in determining the ionization (Pauldrach 1987).

[10] We note that in the BC(T_{eff}) relation given in KHH, a misprint has occurred. The relation should have read: BC = 27.4832 − 6.7985 log T_{eff}.

TABLE 2

PARAMETERS OF THE PROGRAM STARS

	Name	T_{eff} (K)	BC (mag)	V (mag)	$E(B-V)$ (mag)	$\log L$ ($L_\odot$)	R ($R_\odot$)	M_{init} ($M_\odot$)	v_∞ (km s^{-1})	$\log \dot{M}$ ($M_\odot$ yr^{-1})
1	519 A5	43200	−4.03	13.73	0.48	6.03	18.55	76	3000	−4.64
2	509 A7	40700	−3.86	13.73	0.40	5.86	17.20	59	2900	−5.57
3	618	43500	−4.05	14.25	0.47	5.82	14.33	58	3550	−5.17
4	608	43500	−4.05	14.39	0.50	5.80	14.02	57	3750	−4.96
5	535	45000	−4.15	14.49	0.35	5.62	10.57	49	3400	−5.86
6	354	41000	−3.88	14.52	0.37	5.52	11.40	40	2850	−5.71
7	553	42200	−3.96	14.56	0.40	5.58	11.47	44	3150	−5.80
8	508	40600	−3.85	14.51	0.37	5.51	11.53	40	2900	−5.95
9	602	44000	−4.08	14.63	0.50	5.72	12.46	53	3625	−5.44
10	551	45400	−4.18	14.81	0.48	5.66	10.92	51	3150	−5.87
11	533	40400	−3.83	14.81	0.41	5.44	10.66	37	3025	−5.78
12	542	42300	−3.97	14.86	0.43	5.50	10.41	41	3050	−5.75

NOTE.—The given initial masses, M_{init}, are based on the evolutionary tracks of Meynet et al. 1994 for $Z = 0.004$ and increased mass loss. Star R136a-354 is a spectroscopic binary.

turn used to rederive $E(B-V)$ after which a final tuning of the photospheric and wind parameters was done. The final values for the interstellar extinction are given in the sixth column of Table 2. We estimate the error in $E(B-V)$ to be ~ 0.05 mag.

3.5. Terminal and Turbulent Velocity

The blueshifted edge of the C IV $\lambda\lambda 1548$, 1550 doublet has been used to determine the terminal wind velocity. It has been pointed out by Lamers, Cerruti-Sola, & Perinotto (1987) that the edge velocity, v_{edge}, that can be measured from the P Cygni profile needs to be corrected for the effect of wind turbulence. If one neglects to do so, and one identifies the terminal velocity with v_{edge}, one may overestimate the value of v_∞ by some 10%–20%.

We account for turbulence in the formal solution to obtain the theoretical spectrum. The depth dependence of v_{turb} is assumed to be coupled to the flow velocity in such a way that,

$$v_{turb}(r) = \max\left\{v_{turb}^{min}, v_{turb}^{max}\left[\frac{v(r)}{v_\infty}\right]^\gamma\right\}. \qquad (4)$$

We take $v_{turb}^{min} = 20$ km s^{-1} and $v_{turb}^{max} = 0.05 v_\infty$ for all program stars. The latter value is in agreement with turbulent velocities determined by Groenewegen, Lamers, & Pauldrach (1989) for stars of types O7 and earlier. For the power-law dependence, we adopt $\gamma = 1$. Our approach of taking into account line blending (see § 3.3) also allows one to correct for possible inaccuracies in the determination of v_∞ due to the presence of metal lines near the blue edge of C IV. This effect, however, turns out to be of very minor importance. The measured edge velocities are listed in the fourth column of Table 1; the derived terminal velocities are given in the tenth column of Table 2. All v_∞ values have been rounded off into units of 25 km s^{-1}. The typical error is 200 km s^{-1}. In a few cases (including R136a5), the lack of a detailed fitting of v_{turb}^{max} may yield an error as large as 300 km s^{-1}.

3.6. Mass Loss

Mass-loss rates of early-type stars may be derived in several ways (for a recent review, see Lamers & Cassinelli 1996). The most *accurate* diagnostics are free-free emission of the ionized wind at radio wavelengths and the Hα line emission. The most *sensitive* method of determining $\dot{M}$, however, is that of fitting the P Cygni profiles of UV resonance lines. This last method allows for the detection of mass-loss rates as low as log $\dot{M} \sim -8$.

The free-free emission can be used only for stars with considerable mass loss (say log $\dot{M} \gtrsim -6$) at relatively
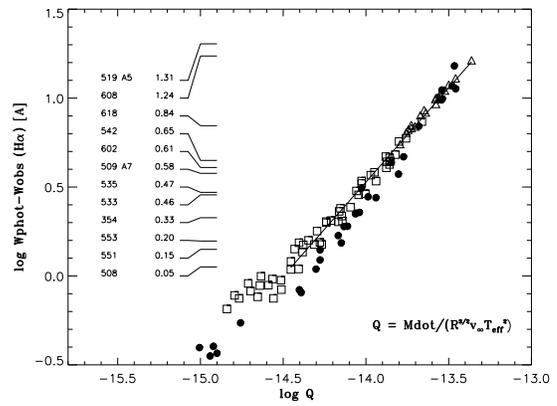

FIG. 4.—Hα + He II $\lambda 6560$ "curve of growth." The models indicated by squares are from the $1\dot{M}_{Gal}$ grid; those designated with triangles are from the $2\dot{M}_{Gal}$ grid. The line is essentially optically thin at an equivalent width invariant $Q < -14.5$. The best fit for the (partly) optically thick case is represented by the solid line. Overplotted are the results for a set of unified atmospheres for O-type stars by the Munich group (*filled circles*; Puls et al. 1996).

nearby distances (say within a few kpc) as otherwise the excess radio flux does not reach present-day detection limits. This eliminates this method for use with the R136a stars. The fitting of UV resonance lines, which in our case would pertain to C IV $\lambda\lambda 1548$, 1550 and N V $\lambda\lambda 1238$, 1242, drops from the list of possible mass-loss diagnostics because the observed lines of the R136a stars are either saturated (C IV in several cases) or are from a minor ionization stage for which the ionization fraction may depend critically on the presence of shocks and X-rays in the wind (N V), processes for which our current models do not account. This leaves the Hα method.

The Hα emission has been used by Leitherer (1988) and Lamers & Leitherer (1993) to derive mass-loss rates of Galactic OB-type stars and by Puls et al. (1996, hereafter P96) for both Galactic and Magellanic Cloud O-type stars. In these papers various approximations have been made regarding the Hα line formation. The most essential assumptions concern (1) the optical thickness of Hα or, more precisely, whether the line may be treated as optically
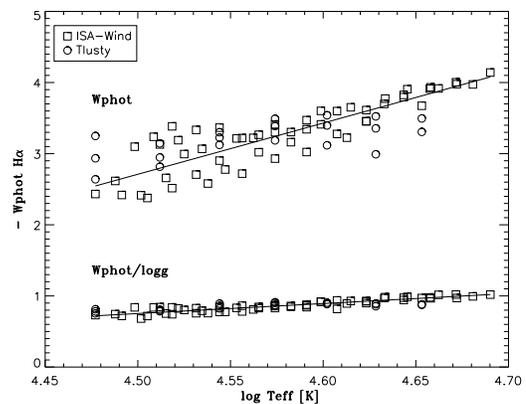
TABLE 3

Hα + He II $\lambda 6560$ EQUIVALENT WIDTHS FOR PLANE-PARALLEL NON-LTE H, He TLUSTY MODELS

T_{eff} (K)	log g					
	3.50	3.75	4.00	4.25	4.50	4.75
30,000......	2.64	2.93	3.25	3.59	3.95	4.35
32,500......	2.82	2.95	3.14	3.40	3.68	4.01
35,000......	3.12	3.23	3.30	3.41	3.57	3.79
37,500......	3.19	3.39	3.49	3.56	3.64	3.74
40,000......	3.12	3.40	3.54	3.62	3.68	3.74
42,500......	2.99	3.36	3.52	3.62	3.68	3.72
45,000......	...	3.31	3.49	3.59	3.65	3.68

NOTE.—Fig. 5 contains TLUSTY results for only log $g \leq 4$.

FIG. 5.—Equivalent width of the photospheric Hα line, W_{phot}. If this quantity is known, one may isolate the (mass-loss–dependent) wind contribution from the observed Hα equivalent width. The squares are for spherical ISA-WIND models in which the mass loss is set to such a low value (10^{-8} $M_\odot$ yr^{-1}) that the profiles are essentially of photospheric origin. For comparison we also give results for plane-parallel TLUSTY models (*circles*). The photospheric equivalent width is derived from the W_{phot}/log g vs. T_{eff} relation, also shown in this figure.

thin; (2) the blending effect of the He II $n = 4 \to 6$ Pickering transition at 6560 Å; and (3) the treatment of the non-LTE departure coefficients of H I $n = 3$ and He II $n = 6$. The validity of all of these has been critically reviewed by P96, to which we refer for a detailed discussion. Gabler et al. (1990), using unified model atmospheres, were the first to develop a general methodology for the Hα diagnostic: the unified model provides the non-LTE populations of both H and He and in the formal solution, which is valid for arbitrary optical depth, the blending of the He II $\lambda6560$ line is treated consistently. We also follow this approach, as does P96.

The Hα + He II $\lambda6560$ "curve of growth" is shown in Figure 4. It shows the *net wind emission*,

$$W_{net} \equiv W_{phot} - W_{obs} , \qquad (5)$$

versus

$$Q \equiv \frac{\dot{M}}{R^{3/2} T_{eff}^2 v_\infty} . \qquad (6)$$

The net emission in Hα + He II $\lambda6560$ follows from the observed equivalent width, W_{obs}, after correction for the (hypothetical) underlying photospheric absorption, $W_{phot}(T_{eff}, \log g)$. The equivalent width invariant, Q, has first been introduced by Schmutz, Hamann, & Wessolowski (1989) for fixed T_{eff}. The dependence of W_{net} on basic parameters is extensively discussed by P96. Their most general result, derived mostly from basic physical arguments, is that $Q \propto R^{-3/2} T_{eff}^{-7/4} v_\infty^{-5/6}$ at about 40 kK. The invariant given in equation (6), however, yielded a marginally tighter relation for the models in our grid than the P96 result. The units of the constituents of Q are $\dot{M}$ in $10^{-6} M_\odot$ yr^{-1}, stellar radius in $R_\odot$, T_{eff} in kelvins, and v_∞ in km s^{-1}.

The models used in Figure 4 are those from the $1\dot{M}_{Gal}$ grid (*squares*), supplemented with those from the $2\dot{M}_{Gal}$ grid (*triangles*) that have $Q > -13.8$ in order to have a good coverage of the relation for cases of relatively high mass loss. The best linear fit relation, also given in the figure, excludes all models having $W_{net} < 1$ Å or $\log \dot{M} < -7$, for which Hα is optically thin and in which case the "curve of growth" has a slope different from the (partly) optically thick case (see P96). The best fit is given by

$$\log W_{net} = 15.360(\pm0.035) + 1.059(\pm0.015) \log Q . \quad (7)$$

For comparison, we have also given the results for the grid of unified atmospheres for O-type stars of Puls et al. (*circles*). Note that the Munich calculations yield a slightly steeper slope at $W_{net} > 1$ Å, which translates to a predicted mass loss up to ~ 0.1 dex higher at the low mass-loss end. A possible cause for this difference may be the use of the Sobolev approximation in our calculations; where P96 solve the line transfer in the comoving frame (see Sellmaier et al. 1993; Santolaya-Rey, Puls, & Herrero 1997). However, a physical reason, such as small differences in the velocity law, can as yet not be excluded. An investigation of the cause of the small discrepancy—which does not affect our conclusions—is beyond the scope of this paper.

Now let us turn to the problem of obtaining the net wind emission. In order to isolate the wind contribution, we need to correct the observed Hα + He II $\lambda6560$ profile for the "photospheric" profile. Note that this W_{net} approach is not really necessary, for one may also derive the mass loss directly from the observed equivalent width. However, the net emission formulation preserves the simple power-law dependence of the "curve of growth" at low mass-loss rates

($\dot{M} \lesssim$ few times $10^{-6} M_\odot$ yr^{-1}). From the practical point, this allows for a more accurate determination of these low mass-loss rates, provided one has a reliable way of predicting the photospheric equivalent width.

To get the W_{phot} values for the Hα + He II $\lambda6560$ profile, we calculated a new set of ISA-WIND models with parameters equal to that of the standard $1\dot{M}_{Gal}$ grid, except for the mass loss, which we set to the very low value of $10^{-8} M_\odot$ yr^{-1}. These models, from here on denoted as the $0\dot{M}_{Gal}$ grid, mimic hydrostatic spherical models. The resulting Hα + He II $\lambda6560$ equivalent widths—which are essentially photospheric—are plotted in Figure 5. For comparison, we also give the theoretical equivalent widths for a set of plane-parallel H, He TLUSTY models. The parameters of this latter grid, together with the corresponding W_{phot} values, are given in Table 3.

Also given in Figure 5 is $W_{phot}/\log g$, which shows only a weak temperature dependence. The best linear fit for all $0\dot{M}_{Gal}$ grid models is given by

$$W_{phot}/\log g = -5.573(\pm0.036) + 1.406(\pm0.084) \log T_{eff} . \qquad (8)$$

In the relevant temperature range ($T_{eff} > 35$ kK say), this relation reproduces the photospheric absorption equivalent width to within 0.2 Å. Neglecting the weak T_{eff} dependence altogether yields for the ISA-WIND models $W_{phot} = 0.864 \pm 0.088 \log g$. This compares very well with the mean value derived for the TLUSTY models, which is $W_{phot} = 0.853 \pm 0.049 \log g$.

Finally, in order to determine W_{phot}, we need to have an estimate of the current stellar mass. To this end, we have derived a mass-luminosity relation from the evolutionary tracks of Meynet et al. (1994) for stars of metallicity $Z = 0.008$ and age 2 Myr. The relation is given by

$$\log (M/M_\odot) = -0.557(\pm0.012) + 0.392(\pm0.012)$$
$$\times \log (L/L_\odot) \qquad (9)$$

and is valid within the current mass range $25 \lesssim M/M_\odot \lesssim 75$. Note that it is not really this estimate of the current mass that determines the typical error in W_{phot}. If the error in mass would be 25%, corresponding to an error in $\log g$ of 0.1 dex, the induced error in W_{phot} will be less than 0.1 Å. The error induced by the use of equation (8) is up to 0.2 Å (see above). We adopt this last value as the typical error in W_{phot}.

This completes the detailed discussion of the modeling strategy as outlined in § 3.2.

4. RESULTS

We applied the modeling strategy discussed in detail in the previous section and tuned the models. The derived photospheric and wind parameters are given in Table 2 (the values for the initial mass, given in this table, will be discussed in § 7.2). The theoretical and observed UV spectra are compared in Figure 6 (thick and thin solid lines, respectively).

4.1. The Derived Effective Temperatures

Let us first focus on the spectral range from 1320 to 1420 Å, containing the O IV $\lambda\lambda1338, 1343$, O V $\lambda1371$, and Si IV $\lambda1394, 1403$ lines. We will no longer concern ourselves with the heavy-metal line spectrum, which is well fitted in all stars. Because all of the program stars have effective temperatures in excess of 40 kK, the theoretical spectra lack
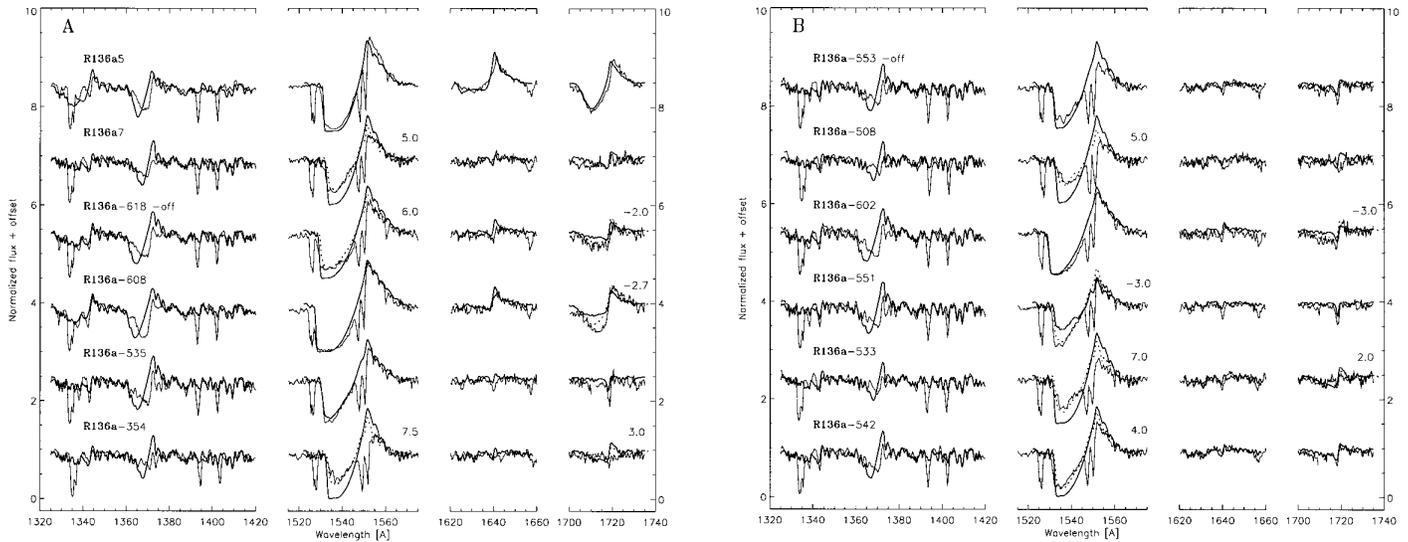
FIG. 6.—Current best fits of the 12 program stars to the GHRS spectra. The horizontal axis is not linear but shows those spectral regions that are used to derive the basic parameters. The thin solid line represents the observations; the thick solid line shows the best-fit model. The dotted line in some of the C IV and N IV profiles represent models at differing $T_{\rm eff}$, but such that these profiles are fitted best. The required shift, $\Delta T_{\rm eff}$, relative to the best fit model is indicated in the plot in kK. Star R136a-354 is a spectroscopic binary. For a discussion, see § 4.1.

pronounced blueshifted or P Cygni–type profiles in Si IV (see § 3.3)—as observed. A photospheric profile for the doublet is predicted, but, obviously, this cannot be verified because of the strong interstellar component of Si IV.

In all but the R136a5 spectrum, the O IV complex fits reasonably well, although this may be somewhat hard to assess for the blue component at λ 1338 Å, which is blended by the interstellar C II $\lambda\lambda$1335 line. As pointed out in § 3.3, we have adopted for all stars the *initial* surface oxygen abundance in the determination of $T_{\rm eff}$. At some point in the evolution, however, CNO-processed material—in which oxygen and carbon are depleted and nitrogen is enriched—will reach the surface layers. The evolutionary age at which to first expect processed CNO, $\tau_{\rm CNO}$, is given in Table 4 for different initial masses, metallicities and mass loss formalisms. The data for the highest mass loss are from recent track calculations by Meynet et al. (1994), in which the main-sequence and WNL-phase mass loss, as given by de Jager, Nieuwenhuijzen, & van der Hucht (1988), is arbitrarily multiplied by a factor of 2. They show that for the most massive stars nuclear processed material will reach the photosphere after some 2 Myr, at which point the oxygen abundance is predicted to drop by about a factor of 30 for stars with $M_i \gtrsim 60\ M_\odot$. The mixing of nuclear burned material toward the stellar surface and wind is a function of

the mass loss assumed. For the most massive stars, an increase in $\dot{M}$ will result in a significant decrease of $\tau_{\rm CNO}$. This can readily be seen from Table 4 by comparing the standard and high mass-loss tracks. As we find mass-loss rates for the R136a stars in excess of what has been assumed by Meynet et al. (see § 5.3), the actual $\tau_{\rm CNO}$ timescales may be even lower. Note that for stars with initial mass $M_i \le 60$ $M_\odot$ and which is what we find for all stars except R136a5 (see § 7.2), the $\tau_{\rm CNO}(\dot{M})$ effect does not appear to be important. An upper limit to the age of R136a of $\tau \sim 2.2$ Myr has been derived by KHH. This limit is based on the finding that even the most massive stars in the cluster, R136a1, R136a2, and R136a3, are still on the main sequence. Such a young cluster age implies that the most luminous, therefore most massive, stars in our sample may have a depleted oxygen abundance.

It is now important to realize that because of our adopted $T_{\rm eff}$ diagnostic, such an oxygen depletion will not show up in the best-fit O V profile (simply because we would have

TABLE 4

EVOLUTIONARY AGE (Myr) AT WHICH FIRST TO EXPECT
CNO-ENRICHED MATERIAL AT THE STELLAR SURFACE

		ZAMS MASS ($M_\odot$)			
METALLICITY	$\dot{M}$	120	85	60	40
$Z = 0.004$......	1x	2.46	3.26	3.90	5.16
	2x	2.04	2.92	3.83	5.11
$Z = 0.008$......	1x	2.19	3.12	3.72	4.92
	2x	1.67	2.73	3.76	4.93

NOTE.—The track calculations assume (1) standard mass loss (Charbonnel et al. 1993; Schaerer et al. 1993) and (2) a main-sequence and WNL-phase mass loss a factor of 2 larger than nominal (Meynet et al. 1994).
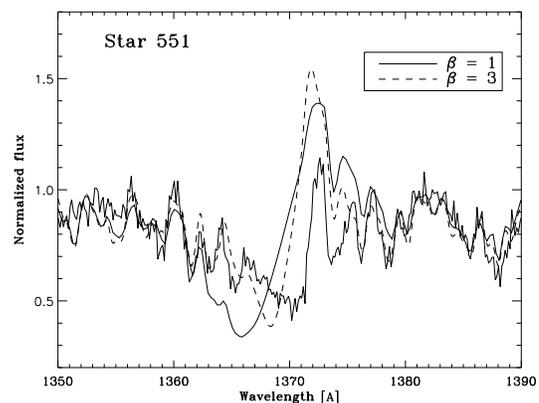

FIG. 7.—Effect of a decrease in the steepness of the velocity law for star R136a-551. The standard value of β is unity. In the $\beta = 3$ model the O V λ1371 line is formed at lower flow velocities. As a consequence (1) the deepest part of the absorption is less blueshifted and (2) part of the metal line spectrum (at $\lambda \lesssim 1367$ Å) is no longer obscured because in the high beta case the O V line is optically thin at corresponding blueshift.

"masked" it by a temperature that is too high; see § 3.3). However, in O IV, which is also sensitive to mass loss, an overestimate in the abundance will produce a line profile that is too strong. This is the case for R136a5 and confirms the result of de Koter et al. (1997), who found an oxygen depletion of about a factor of 10 for this star. Their derived temperature of $T_{eff} = 42.4$ kK is therefore lower than the 43.2 kK derived here. None of the other stars show a value of O IV that is too strong. We conclude that for none of the program stars, except R136a5, the T_{eff} determination is corrupted by a incorrect assumption on the oxygen abundance.

The most crucial line in the wavelength range from 1320 to 1420 Å is O V $\lambda1371$. Figure 6 shows that—although the absorption equivalent widths of the theoretical and observed profiles match—the profile shapes do not agree well. The theoretical absorption is more blueshifted, while the emission is generally predicted too strong.

One might argue that the discrepancy in the absorption is caused by an adopted velocity law that is too steep, for if the velocity law would be slower, an equal density would correspond to a lower wind velocity. Figure 7 shows the effect of an increased β (decreased steepness) for star 551. The standard β case of unity is also given. Indeed, a value of $\beta = 3$ yields a blueshift of the deepest part of the absorption, which is some 500 km s^{-1} less than the default β case. Also, one essentially recovers the part of the metal line spectrum at $\lambda \lesssim 1367$ Å that in the $\beta = 1$ model is obscured by optically thick blueshifted O V absorption at flow velocities $v \gtrsim$ 900 km s^{-1}.

Nevertheless, we do not expect that the discrepancy in the O V fit is properly explained by the above argument. The reasons are as follows: (1) The profile fits to other UV and optical wind lines become worse. (2) Although the fit to the observed absorption is markedly improved in the higher β case, the fit to the emission grows worse as for a slower accelerating wind the emission close to line center is increased. (3) A β value substantially larger than unity is hard to reconcile with theoretical predictions of the wind acceleration. For radiation-driven winds of Galactic O stars in the T_{eff} range from 40 to 50 kK, Pauldrach, Puls, & Kudritzki (1986) found that $\beta \simeq 0.8$. This value is in reasonable agreement with observations (Groenewegen & Lamers 1989). Note that high β values may be expected theoretically, but typically for winds in which multiple scattering effects are important (Springmann 1994; Gayley, Owocki, & Cranmer 1995). This is also confirmed by observations; for instance, KHH derived values of $\beta = 1.25$ and 2 for the Wolf-Rayet–like stars R136a1 and R136a3, respectively.

A simpler explanation of the O V discrepancy is that the line is formed closer to the star than is predicted. In that case, for obvious reasons, the absorption would occur at lower velocities. That the emission decreases is understood by realizing that the O V line is mostly optically thick.[11] In this case, the decrease in line emission is due to a smaller projected area of the emitting surface. That we predict a line formation region that is too large may be connected to the neglect of metal line blanketing effects in our models (see § 3.3 for a discussion).

---

[11] The P Cygni character of the predicted O V $\lambda1371$ line is a result of the strong coupling of the lower $2p$ $^1P^o$ level to the ground level and because the $2p$ $^1P^o$–$2p$ $^2D^e$ transition itself remains optically thick out to ~ 1.5 stellar radii.

Let us now turn to the fits of the C IV $\lambda\lambda1548$, 1550 and N IV $\lambda1718$ profiles. About half of the predicted profiles give good fits to the observations. Of the other half, the theoretical C IV profiles are, generally, too strong, while some of the N IV predictions yield lines that are either too weak or too strong. One may argue that these discrepancies provide a measure of the quality of our O V temperature calibration. The temperature shifts, ΔT_{eff}, required to recover proper fits to the deviating C IV and N IV profiles are labeled in units of kK in Figure 6. The predicted profiles for these adjusted temperatures are given by the dotted lines. Note that when changing T_{eff} in the model, we modified other basic parameters such that visual magnitude and equivalent width invariant Q (eq. [6]) were conserved. In the case of N IV, a change in T_{eff} by typically 0.02–0.03 dex was necessary to fit the profile properly. This amounts to the characteristic accuracy in temperature determination of Galactic O-type stars (see Voels et al. 1989; Herrero et al. 1992; Kudritzki et al. 1992; Herrero 1994). The discrepancy in C IV is about twice as large and, in six of seven cases, requires an adjustment toward higher T_{eff}. This likely points to a systematic effect, again, possibly connected to the neglect of line blanketing in our models (but now it requires a *more* effective reionization at about the sonic point, where C V becomes the dominant ion in all relevant models).

Another possibility is that the carbon abundance, A_c, is systematically overestimated. To fit the lines properly requires a decrease in carbon abundance from about a factor of 5 (star 542) up to a factor of ~ 20 (star R136a-354). At the same time, one needs to increase the terminal flow velocity by ~ 250 to 350 km s^{-1}. As a reference, the Meynet et al. (1994) evolution scenarios predict a decrease in carbon abundance of about a factor of 15–20 when nuclear processed material reaches the surface layers. As discussed above (in the case of oxygen), we cannot exclude the possibility that the CNO surface abundances of some of the stars have deviated from their initial values. However, at this point, this cannot be discerned from an imperfection in the predicted carbon ionization stratification.

In summary: the temperatures of the program stars are high, between $T_{eff} \simeq 40$ and 46 kK. The standard deviation in the derived effective temperatures is about 0.02 to 0.03 dex. Again, a systematic shift in the scale extending perhaps even up to ~ 0.05 dex toward higher temperatures—due to effects related to the neglect of metal line blanketing—cannot be entirely excluded (see § 3.3).

4.2. *The Derived Mass-Loss Rates*

The mass loss has been derived from fitting the hybrid Hα + He II $\lambda6560$ profile (see § 3.6). The best-fit profiles are given in Figure 8. The line list used for this spectral range contained lines of hydrogen and helium only. The thick and thin solid lines represent the theoretical and observed spectra, respectively. All predictions yield a reasonably good fit. In most cases the line shows a photospheric profile in which wind emission fills in the central part. In the highest mass-loss cases (such as for stars R136a5 and R136a-608) the line is completely in emission. In the spectral range shown in Figure 8, we also predict a weak He II $\lambda6527$ profile; however, the quality of the observations is too low to identify this line reliably.

The He II $\lambda1640$ profile may also be used as a mass loss indicator. A comparison of predicted and observed profiles is given in Figure 6 (see above). For the stars with the
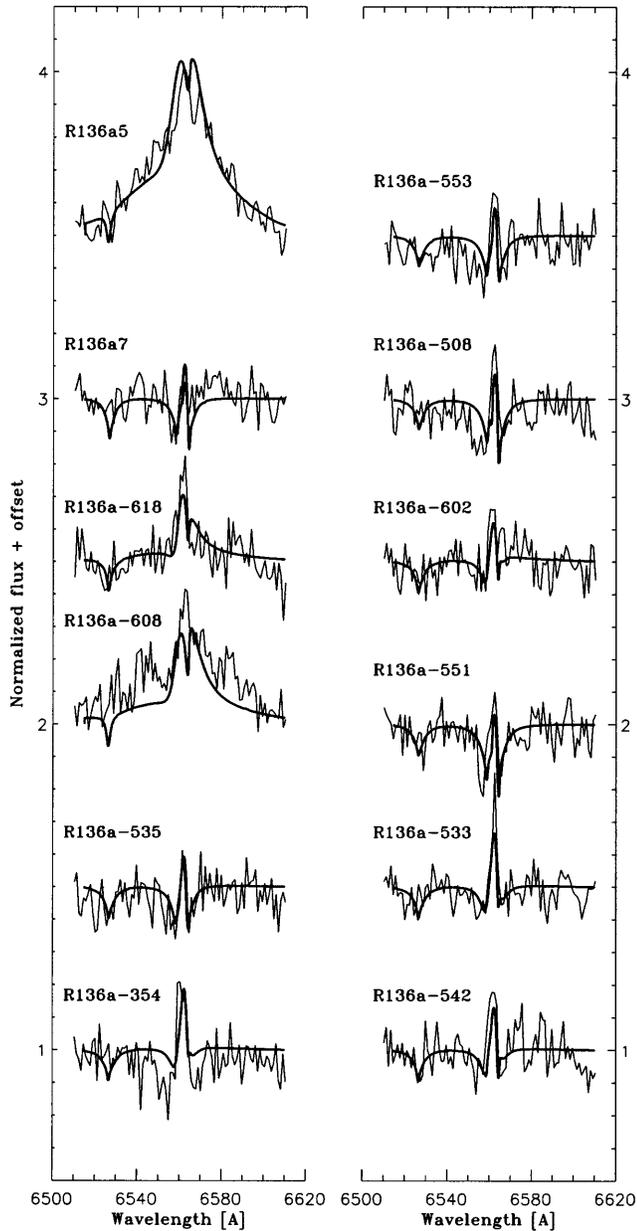
FIG. 8.—Current best fits of the Hα + He II λ6560 line for all 12 program stars. The observations are taken with the FOS. The theoretical and observed spectra are given by the thin and thick solid lines, respectively. The stars are given in the same order as in Fig. 6. For a discussion, see § 4.2.

densest winds, such as stars R136a5 and R136a-608, this line is fully in emission. For the lower mass-loss rates, the line is mostly in absorption, which makes it somewhat difficult to judge the quality of the fit owing to the presence of many metal lines. However, in all cases the line fits reasonably well, and for none of the stars does it lead to contradictory conclusions regarding the mass loss derived from Hα.

In the case of star R136a5, the strong Hα + He II λ6560 and He II λ1640 lines may be used to check the assumption of a solar hydrogen to helium abundance ratio. The assumption seems valid as both lines are fitted correctly by $n(\mathrm{He/H}) = 0.10$. This diagnostic can not be used (as) reliably for the other, lower luminosity—therefore lower $\dot{M}$—stars in our sample. However, assuming an instantaneous burst

of star formation in R136a, one may expect that these stars with lower initial mass have likewise initial H/He-ratios.

5. THE DEPENDENCE OF MASS LOSS ON STELLAR PARAMETERS

In this section, we will compare our derived mass-loss rates with results of other O-type star analyses. Ideally, one would like to compare the observed $\dot{M}$ values of stars with equal metallicity, as it is theoretically expected that mass loss is dependent on Z (see, e.g., Kudritzki et al. 1987). However, for only a few other stars in the LMC have reliable mass-loss rates been determined. Therefore, we will also compare our derived rates with those found for Galactic stars. Such an approach remains meaningful because it allows us to investigate whether a similar or different dependence of mass loss on stellar parameters holds for very massive members of R136a compared to Galactic O stars.

We will do the $\dot{M}$ comparison in three ways: first, by looking at the mass loss versus luminosity relation; second, by investigating the wind momentum–luminosity function; and third, by comparing $\dot{M}(L, T_{\mathrm{eff}})$ representations.

5.1. Mass Loss versus Luminosity Relation

Figure 9 shows the mass loss versus luminosity relation for the R136a stars. The filled circles represent the results of the present study; the shaded circles denote the Wolf-Rayet–like stars R136a1 and R136a3 and the Of/WN-type stars R136a5 and Melnick 42, investigated by KHH. For the one star examined in both papers, R136a5, the derived mass-loss values agree well; the difference in luminosity is due almost solely to a difference of 0.13 in derived extinction. We derive a mass loss versus luminosity relation

$$\log \dot{M} = -16.57(\pm 0.22) + 1.94(\pm 0.20) \log (L/L_\odot) . \quad (10)$$

The mass-loss unit is $M_\odot$ yr^{-1}. The binary R136a-354 and the R136a5 point of KHH have been excluded in the derivation of this relation. The $\dot{M}$-L relation for Galactic O-type stars (squares), derived from the results of the Puls et al.
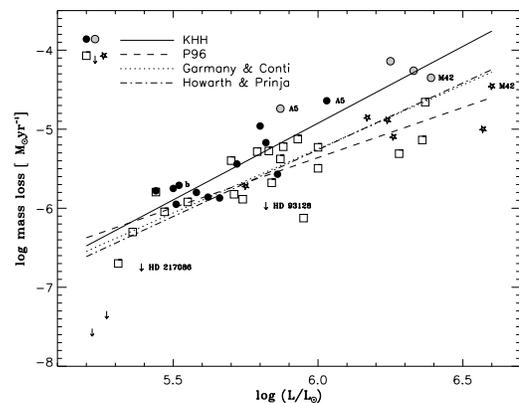

FIG. 9.—Comparison of our mass loss vs. luminosity relation with the one derived by P96. The filled circles are the data for the stars investigated here. In deriving the best fit (solid line), we added the three Wolf-Rayet–like stars and Melnick 42 investigated by KHH. The squares (stars) denote the P96 results for Galactic (LMC) stars. The downward-pointing arrows indicate stars for which they obtained only upper limits. The best fit to the Puls et al. data only uses the Galactic stars (dashed line). The label "b" indicates the binary R136a-354. Also given are $\dot{M}$-L relations from Garmany & Conti (1984) and Howard & Prinja (1989).

(1996) study, is also given. In their case, one finds

$$\log \dot{M} = -12.97(\pm 0.29) + 1.27(\pm 0.22) \log (L/L_\odot) \, . \quad (11)$$

Note that the LMC stars (stars) investigated by P96 seem to follow about the same best-fit representation. In comparing the results, one sees that the relations more or less meet at luminosities $\log (L/L_\odot) \lesssim -5.5$. However, because of the steeper luminosity dependence of the R136a stars, they diverge toward higher L values. As we will point out in the next section, the agreement at relatively low L is somewhat misleading as it does not compare stars in the same part of the Hertzsprung-Russell diagram. For the highest luminosity stars, the difference between the two fit curves increases to about a factor of 6. One reason for the steeper dependence may be connected to the $T_{\rm eff}$ determination of the highest luminosity stars. We illustrate this using the one star in our sample in common with P96, namely Melnick 42 (indicated by M42 in Fig. 9). The $\dot{M}$ values derived by the Goddard and Munich groups are very similar; however, the latter find a temperature that is 6 kK higher than the KHH value of $T_{\rm eff} = 44.5$ kK. Possible causes for this discrepancy have been addressed in § 3.3. The corresponding difference in bolometric corrections implies a shift in luminosity of ~ 0.15 dex (see eq. [3]). Applying the appropriate shift to the very brightest stars—say for those having $\log (L/L_\odot) \gtrsim 6$—in the results of either the Goddard or Munich group brings the respective slopes of the $\dot{M}$-L relation in significant better agreement.

Also given in the figure are the $\dot{M}$-L relations published by Garmany & Conti (1984) and by Howarth & Prinja (1989). The slopes of these relations (1.62 and 1.69, respectively) are more similar to what we find. The discrepancy in the derived mass loss at relatively high luminosity is also somewhat smaller.

5.2. Wind Momentum versus Luminosity Relation

A comparison of observed mass-loss rates by looking at the $\dot{M}$-L relation neglects the possibility that mass loss may also depend on other stellar parameters. For instance, the theory of radiation-driven wind shows that both the individual quantities mass loss and terminal velocity are rather sensitive functions of the stellar mass. This can readily be seen from the analytical solution of the line-driven wind problem as formulated by Kudritzki et al. (1989). Interestingly, a further investigation of the analytical wind momentum solution reveals a quantity that is almost *independent* of stellar mass (P96). This quantity is $\dot{M}v_\infty R_*^{0.5}$ and is referred to as the modified wind momentum. Indeed, the wind momentum versus luminosity relation was already found empirically by Kudritzki, Lennon, & Puls (1995), who presented observational evidence of this correlation using a large sample of Galactic giant and supergiant OBA stars.

The wind momentum–luminosity relation for the program stars is given in Figure 10, together with the results of P96. The symbols have meanings identical to those in the mass loss–luminosity plot Figure 9. Note the similarity between Figures 9 and 10. This is mainly a consequence of the finding that all program stars have more-or-less similar v_∞ (see Table 2). The theory of line-driven winds also predicts the terminal velocity to be almost proportional to the surface escape velocity, the proportionality constant being about 2.6 for O-type stars (Lamers et al. 1995). In order to estimate $v_{\rm esc}$, let us adopt the initial mass derived from a
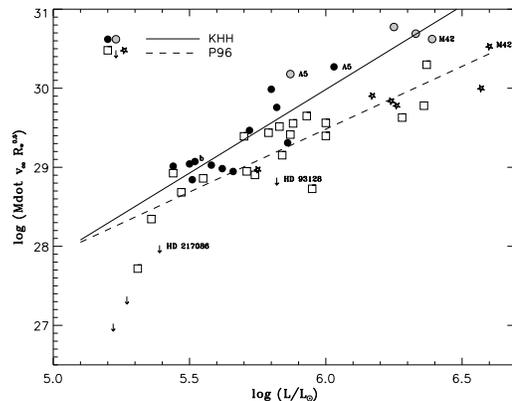

FIG. 10.—Comparison of our wind momentum vs. luminosity relation with the one derived by P96. See Fig. 9 for an explanation of the symbols and line styles. The best-fit curve for our data points is given by $\log \dot{M}v_\infty R_*^{0.5} = 17.29(\pm 0.24) + 2.12(\pm 0.21) \log (L/L_\odot)$; for the P96 points we find $\log \dot{M}v_\infty R_*^{0.5} = 19.94(\pm 0.31) + 1.56(\pm 0.23) \log (L/L_\odot)$.

comparison with evolutionary tracks (see Table 2 and § 7.2) as indicative of the current mass. In § 7.2, we will point out that this assumption is reasonable for stars initially less massive than ~ 50 $M_\odot$. For stars initially more massive, this assumption overestimates the current mass. The escape velocities derived in this way all are in the range $1150 \lesssim v_{\rm esc} \lesssim 1350$ km s^{-1}. This relatively narrow range in $v_{\rm esc}$ helps explain the rather similar observed terminal velocities.

Given in Figure 10 are the best-fit curves for both our and the P96 data. The same points are used as in Figure 9. The behavior of the best-fit lines is comparable to those in the mass loss–luminosity plot, and the same argument as to the possible cause of the difference applies.

5.3. Mass Loss in the Hertzsprung-Russell Diagram

Multidimensional parameterizations of the mass loss usually limit the dependency to L and $T_{\rm eff}$. Higher dimensional fits do not appear to decrease the standard deviation of individual mass-loss rates further, which hints that the accuracy of such fits is predominantly limited by the errors associated with deriving $\dot{M}$ and not by additional functional dependencies (Lamers & Leitherer 1994). In a two-dimensional parametrization, one is obviously not compelled to represent mass loss as $\dot{M}(L, T_{\rm eff})$. For instance, Lamers & Cassinelli (1996) present a formula that essentially models $\dot{M}$ as a function of luminosity and mass.[12] The drawback of such an adopted dependence is that it includes a parameter (stellar mass) that—as yet—cannot be determined accurately by spectroscopic analysis. This prevents a direct comparison of our results with those of Lamers & Cassinelli.

The stellar evolution track calculations of the Geneva group have made extensive use of the mass-loss parameterization of de Jager et al. (1988); see, for example, Schaller et al. (1992). The de Jager et al. relation is used for all evolution phases of stars with nonnegligible mass loss, up to the Wolf-Rayet stage. Recently, Meynet et al. (1994) published tracks in which the de Jager et al. mass-loss values, henceforth $\dot{M}_{jnh}$, for stars on the main sequence have been multiplied by a factor of 2. In Figure 11, we compare our results with these multiplied $\dot{M}$ values for metallicity

---

[12] In representing mass loss as a function of L and M, one essentially absorbs the $T_{\rm eff}$ dependence in the stellar mass.
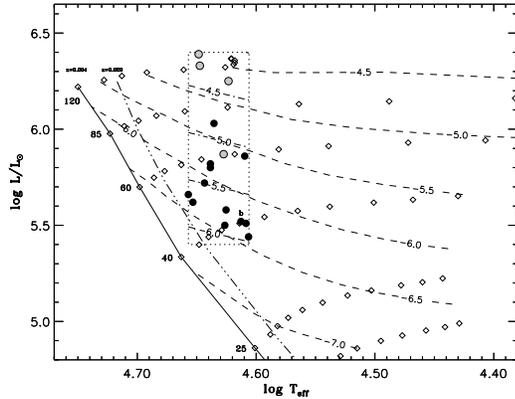
FIG. 11.—Comparison of our $\dot{M}(L,T_{\rm eff})$ representation with that of de Jager et al., for which contours of equal mass loss are given by the dashed lines (labels give log $\dot{M}$). The validity range of our results is indicated by the dotted box; contours by the dot-dashed-dashed lines. The de Jager et al. mass-loss rates are for a metallicity $Z = 0.004$. Models along the evolutionary tracks of different initial masses are given by the shaded squares. The solid line represents the ZAMS; initial masses along this isochrone are labeled. For comparison, we also give the ZAMS for $Z = 0.020$ (triple-dot–dashed line). See text for a discussion.

$Z = 0.004$. For the Chebychev $\dot{M}_{jnh}$ representation, contours of equal mass loss are represented by dashed lines and are labeled by their respective log $\dot{M}$ values. In a strict sense, the dotted box indicates the range of validity of our $\dot{M}(L,T_{\rm eff})$ formula; contours are given by the dot-dashed-dashed lines. We find

$$\log \dot{M} = -2.83(\pm 0.22) + 2.04(\pm 0.20) \log (L/L_\odot)$$
$$- 3.08(\pm 3.85) \log T_{\rm eff} . \qquad (12)$$

The absolute mean deviation of the data points around this relation is 0.18 dex. The large error in $T_{\rm eff}$ dependence is due to the small temperature baseline and prevents one from drawing reliable conclusions regarding this dependence. Looking at a representative $T_{\rm eff}$ value of 42.5 kK for the R136a stars, one sees that the mass loss on luminosity dependence is only marginally weaker in the de Jager et al. formula compared to the power-law index of 2.04 that we derive. A surprising difference, however, is that *the mass loss*
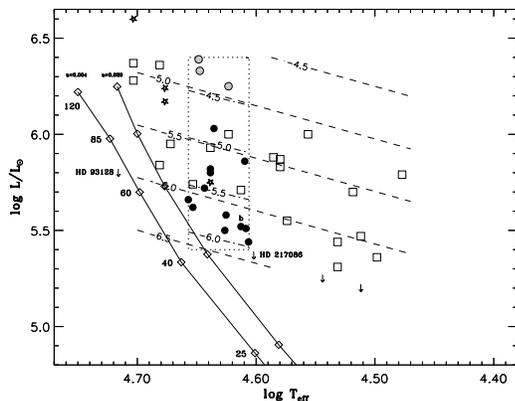

FIG. 12.—Comparison of our $\dot{M}(L,T_{\rm eff})$ representation with that of P96. The symbols have the same meaning as in Fig. 9. Notice that now the downward-pointing arrow denotes stars at the given H-R position for which P96 could determine only an upper limit value of $\dot{M}$. The basic parameters derived for HD 93128 imply a position below the ZAMS. The puzzling character of this star has already been noted by Conti & Burnichon (1975), Simon et al. (1983), and Kudritzki et al. (1992).

of the most massive R136a stars is ~ 0.3–0.5 *dex higher than the scaled* $Z = 0.004$ *rates and* ~ 0.15–0.35 *dex higher than the scaled* $Z = 0.008$ *rates.*

At this point we would like to point out that the rather strong $T_{\rm eff}$ dependence of the 20 term Chebychev adaptation of de Jager et al. leads to relatively low $\dot{M}$ values near the main sequence—especially for stars of low metallicity. One should bear in mind that their representation is valid only for Galactic stars and is simply scaled for LMC metallicities. Moreover, the relatively steep fall in $\dot{M}$ is extrapolated toward higher $T_{\rm eff}$ and is therefore most notable for the hotter ZAMS stars at lower Z. This procedure may cause one to underestimate the mass-loss rate significantly for stars near the ZAMS in tracks for low metallicity environments.

The mass loss–luminosity relation presented in Figure 9 suggests that for the relatively low luminosity stars, say at $\log (L/L_\odot) \lesssim 5.5$, the average R136a $\dot{M}$ values are comparable to those of Galactic O-type stars. In Figure 12 we show that in this respect, the mass loss versus luminosity relation is somewhat misleading. In the figure, we again compare our results with those of P96 but now by plotting the two-dimensional representation $\dot{M} = a + b \times \log (L/L_\odot) + c \times \log T_{\rm eff}$ in the H-R diagram. For the Galactic Puls et al. results, we recovered $a = -1.714(\pm 0.253)$, $b = 1.829(\pm 0.291)$, and $c = -3.160(\pm 1.233)$. The plot symbols have meanings identical to those in Figure 9.

The temperature dependence in P96 is identical to that for the R136a stars. Turning to the stars at $\log (L/L_\odot) \lesssim 5.5$, one sees that the investigated Galactic ones have systematically lower temperatures: the R136a stars range between $T_{\rm eff} \sim 40$ and 46 kK; the Galactic stars range between $T_{\rm eff} \sim 31$ and 35 kK. Comparison of the best-fit relations at $T_{\rm eff} = 42.5$ kK and $\log (L/L_\odot) = 5.4$ shows that even the relatively low luminosity stars in our sample have a mass loss about 0.4 dex higher than Galactic stars at the same position in the H-R diagram. [The only Galactic star that may be used for a direct comparison is HD 217086, for which P96 derive $T_{\rm eff} = 40$ kK; $\log (L/L_\odot) = 5.39$ and an upper limit to the mass loss of $\log \dot{M} \lesssim -6.7$. At the same position in the H-R diagram, our mass-loss representation yields $\log \dot{M} \simeq -6.1$.] This shows that one should be somewhat careful when interpreting a mass-loss estimate in terms of a luminosity dependent only.

6. COMPARISON OF THE OBSERVED MASS LOSS WITH THEORETICAL PREDICTIONS

It is interesting to see how the observationally derived $\dot{M}$ values compare with mass loss as predicted by radiation-driven wind theory. We approach this question in the following way.

We use the analytical solution for radiation-driven winds of Kudritzki et al. (1989) to predict mass-loss rates and terminal velocities. In this analytical formulation, the radiative acceleration on spectral lines is expressed in terms of distance-independent force multiplier parameters, denoted k, α, and δ, first introduced by Castor, Abbott, & Klein (1975) and Abbott (1982). The force multipliers depend on metallicity as Z affects the total number of effective lines—represented by k—as well as the distribution of effectively strong and weak lines—represented by α. In principle, k, α, and δ are also dependent on basic stellar parameters. Ideally, the values of the force multipliers should be obtained from detailed non-LTE calculations. Pauldrach et
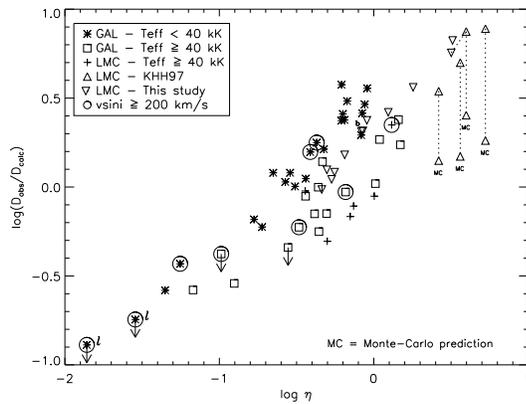
FIG. 13.—Comparison between observed and predicted wind momentum rate ($D = \dot{M}v_\infty R^{0.5}$) vs. observed performance number η. The data are from P96 for Galactic and LMC supergiants. The star symbols denote stars with $T_{\rm eff} \geq 40$ kK; squares represent $T_{\rm eff} < 40$ kK. The plus signs are for LMC stars. Upward-pointing triangles indicate the R136a stars investigated by KHH; downward-pointing triangles represent stars investigated in this study. Mass-loss rates are predicted following P96 unless they are labeled MC, in which case they are predicted following KHH.

al. (1990) were the first to calculate force parameters for a grid of massive stars of Galactic metallicity, based on a solution of the full multilevel non-LTE problem. Since 1990, the detailed physics ingredients of the Munich wind code have been improved significantly and new case specific k, α, and δ values have been derived (PKPBH; P96; Taresch et al. 1997). A new grid of values has not yet been published. Using the (somewhat outdated) Pauldrach et al. (1990) results at face value, one sees that in the range of $T_{\rm eff}$ from ~ 33 to 51 kK and effective gravities between 2.42 and 3.82, k and α are almost constant. Qualitatively, this behavior is typically explained by the argument that at these $T_{\rm eff}$'s the total driving force is composed of lines of different ions of many elements. A different temperature may yield a somewhat different ionization of certain chemical species, but the net effect of all these changes on $\dot{M}$ will be small[13] (Leitherer et al. 1989; de Koter 1997). The Pauldrach et al. (1990) models do show considerable variation in the ionization balance throughout the wind—represented by δ—but fortunately this has little effect on the predicted values for $\dot{M}$.

We adopt the force multiplier values for Melnick 42, as derived by Pauldrach et al. (1994). Melnick 42 is an O3 If/WN–type star and a member of the 30 Doradus cluster (NGC 2070). The star is only at some 8″ distance from the core of R136a. Pauldrach et al. assume a metallicity $Z = 0.004$ for this star and find $k = 0.065$, $\alpha = 0.70$, and $\delta = 0.08$. The way we have applied the theory of radiation-driven winds is to use the observed terminal velocity and other basic parameters to predict mass loss and stellar mass (see § 5.2). To compare with the predictions, we follow P96 in concentrating on the wind momentum rate $D_{\rm calc} = \dot{M}v_\infty R_*^{0.5}$. Note that mass loss is the only theoretical value in $D_{\rm calc}$. Figure 13 shows the difference between the observed and predicted momentum rate versus observed performance number $\eta = \dot{M}v_\infty/(L/c)$. Included in the figure are results from different studies. Note the systematic discrepancy between theory and observations, first detected by Lamers & Leitherer (1993). At large performance numbers, the theory underestimates the mass loss, while at small η, it overestimates $\dot{M}$. The defect of the theory at large η is generally attributed to the neglect of effects of multiple photon momentum transfer (see Lucy & Abbott 1993; Springmann 1994; P96). This has been confirmed by KHH. At small η, the theory may fail because of an inadequate treatment of line overlap or multiline effects (P96).

In Figure 13, the data for Galactic and LMC field stars are from P96. Details are given in the legend. The triangles indicate stars in the R136a cluster. The upward-pointing ones are for stars R136a1, R136a3, R136a5, and Melnick 42, investigated by KHH. Those without the label MC are calculated using mass-loss rates predicted by radiation-driven wind theory; those with the label MC result from Monte Carlo simulations in which the effects of multiple photon momentum transfer are accounted for (for details, see KHH). The downward-pointing triangles denote the program stars. (The two connected symbols are both for R136a5.) Our stars follow the gradual increase of the discrepancy. For relatively small η, observed and predicted wind momentum agree well. For relatively large η, our program stars "connect" to the high mass-loss Wolf-Rayet–like stars R136a1 and R136a3.

The KHH results including multiple photon scattering processes (labeled MC) show that the main cause of the discrepancy is likely due to the neglect of these effects in the derivation of k, α, and δ. However, to what extend may the difference be attributed to errors in the adopted force parameter values *not related* to multiple photon momentum transfer? We point out two such possibilities: First, one should realize that the force multiplier parameters of Melnick 42 have been derived from a self-consistent wind model that has $\dot{M} = 2.7\ 10^{-5}\ M_\odot\ {\rm yr}^{-1}$. So the k, α, and δ numbers are just those that reproduce this mass loss (and the observed v_∞). P96 updated the Melnick 42 mass loss to $3.5 \times 10^{-5}\ M_\odot\ {\rm yr}^{-1}$. Moreover, KHH found $\dot{M} = 4.5 \times 10^{-5}\ M_\odot\ {\rm yr}^{-1}$. This implies that the adopted force multipliers underestimate the mass loss by ~ 0.1 to 0.2 dex. Second, Pauldrach et al. derive a rather high effective temperature, consequently high luminosity, for Melnick 42 (see § 3.3). Let us assume for a moment that this $T_{\rm eff}$ is overestimated. This would yield a value that is too high for the luminosity and would imply that k, and consequently our predicted $\dot{M}$ rates, have been underestimated.

It may be interesting to see whether significant changes occur in the predicted mass loss if we adopt the force multipliers for the Galactic O3 If* supergiant HD 93129A, determined by Taresch et al. (1997). The advantage of using these values is that they represent the most recent level of development of the Munich wind code (improvements relative to PKPBH include the use of the Sobolev approximation with continuum, updates to the line list and atomic models, and a better treatment of shock emission). They have the disadvantage that they have been calculated for a $T_{\rm eff} = 52$ kK, which is even higher than the 50.5 kK derived for Melnick 42, and that they are calculated for solar abundances. As the LMC metallicity is not expected to be much different from the Galactic one (see, e.g., Haser et al. 1998), the latter will introduce only a modest systematic error in

[13] At lower temperatures, say at $T_{\rm eff} \lesssim 25$ kK , the driving force is mainly supplied by only few ions of iron and nickel, yielding a more pronounced dependence of mass loss on temperature.

the predicted wind momentum that may be corrected for using the mass loss–metallicity scaling law (see, e.g., P96). Taresch et al. derive $k = 0.141$, $\alpha = 0.62$, and $\delta = 0.06$. Applying these values, we find that the predicted mass loss increases up to a maximum of only 0.06 dex *before scaling*. Adopting the most favorable value for the LMC metallicity, $Z = \frac{4}{5} Z_\odot$ (Haser et al. 1998) and applying a scaling law $\dot{M} \propto Z^{0.68}$ (following P96), we need to shift the wind momentum by -0.07 dex. We conclude that the use of the Taresch et al. force multipliers would not significantly alter the predicted wind momentum.

7. SUMMARY AND DISCUSSION

In this paper, we have presented a spectroscopic analysis of 12 stars in the dense cluster R136a, the main ionizing source of the 30 Doradus nebula in the LMC. All 12 of these stars are located within $2''$ of the center of the cluster and are its brightest members save for three Wolf-Rayet–like O3-type stars of which a spectroscopic analysis has been presented by KHH. The most outstanding new results of this study are the following:

1. All save one of the investigated stars, which span a luminosity range of a factor of 4, have the *same* spectral type, namely O3, which is the earliest spectral type defined. One star has type O4. Although the spectral type O3 allows for a wide range in temperatures—from say about 40 kK to much higher—the derived values occupy only the relatively small range in temperature from $T_{\rm eff} \sim 40$ to 46 kK.

2. The mass-loss rates for the least luminous stars in our sample—at $\log(L/L_\odot) \sim 5.5$—agree with the predictions of radiation-driven wind theory (Kudritzki et al. 1989); however, for increasing luminosity, the observed mass loss becomes larger, reaching up to 3–4 times what is expected from theory at $\log(L/L_\odot) \simeq 6.0$. This trend is consistent with the study of the very brightest stars in this cluster, R136a1, R136a2, and R136a3 by KHH, where discrepancies of up to a factor of 8 between observed and predicted mass loss are found. The increasing discrepancy is also present as a function of wind performance number η, i.e., as a function of the ratio between stellar wind and photon momentum flux. This defect in the theory is generally attributed to the neglect of effects of multiple photon momentum transfer (Lucy & Abbott 1993; Springmann 1994; P96) and which has been confirmed by KHH.

Compared to $\dot{M}$ rates used in current evolutionary track calculations (Meynet et al. 1994), our observed mass-loss rates are 0.3–0.5 dex higher for an LMC metallicity $Z = 0.004$ and 0.15–0.35 dex higher for $Z = 0.008$.

3. Concerning the spectroscopic diagnostics: (*a*) We have found that the strength of the O v $\lambda1371$ line can be used as a good starting point for the determination of $T_{\rm eff}$. One should, however, be careful to correct for the presence of photospheric and subsonic metal lines. Although the O v method appears very promising, it should be noted that we can not completely exclude that the neglect of a consistent treatment of line blanketing in our ISA-WIND models might introduce a systematic error in effective temperature as large as 0.05 dex. (*b*) We have shown that a relatively simple way to model the blending by UV metal lines is a generalized form of the "modified nebular approximation" (Schmutz 1991) in the formal solution. In the spectral range

around the O v $\lambda1371$ line (i.e., from 1320 to 1420 Å) we achieved satisfactory fits for all 12 program stars. (*c*) We use a consistent treatment of the Hα method of determining mass loss. Hα is viewed as the most reliable $\dot{M}$ diagnostic for distant O-type stars (see P96). A unified model provides the non-LTE level populations of both H and He, and in the formal solution, valid for arbitrary optical depth, the blending of the He II $\lambda6560$ is treated consistently.

In the remaining part of this section, we will discuss the implication of our new results in the context of stellar evolution.

7.1. *First Empirical Isochrone of Very Massive Stars*

The 12 stars of our sample constitute an empirical isochrone of young very massive stars in the H-R diagram. There are three reasons that R136a is the ideal object to define such an isochrone: (1) Perhaps with the exception of the highly reddened Galactic cluster NGC 3603, it is the only resolved cluster rich enough in very massive stars. For instance, from Malumuth & Heap (1994) one may estimate that there are some 200 stars more massive than 10 $M_\odot$, and there are at least a dozen stars with $M \gtrsim 40\ M_\odot$. (2) The observed stars, including those investigated by KHH, cover a substantial range in initial masses, say from $M_i \sim 35$ to 130 $M_\odot$, and luminosities, say from $\log(L/L_\odot) \sim 5.4$ to 6.4. (3) R136a has a very compact size; its radius is about $3''$ or 0.75 pc at the distance of the LMC. This implies a sound-crossing time of only $\sim 100{,}000$ yr; consequently, the 12 program stars can be considered to have been formed simultaneously. (4) The distance to the LMC is well known.

Figure 14 shows the upper part of the H-R diagram in which we compare the location of the program stars with the isochrones for 0, 1, 2, and 3 Myr of the Meynet et al. (1994) tracks for $Z = 0.004$. The temperatures of all stars are assigned a standard deviation $\Delta \log T_{\rm eff} = 0.025$. The slope of the plotted error bars show how the luminosity varies within $T_{\rm eff} \pm \Delta T_{\rm eff}$ owing to the changing bolometric correction. The stars cluster around an age slightly above 2 Myr, although they do not strictly coincide with a single
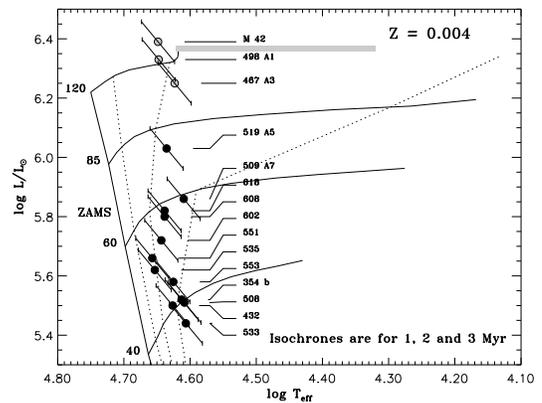

FIG. 14.—Comparison of the empirical isochrone defined by the program stars with predicted isochrones by Meynet et al. (1994). The tracks used are for a metallicity $Z = 0.004$ and a main-sequence mass loss multiplied by a factor of 2. The shaded bar for the track of initial mass 120 $M_\odot$ indicates a main-sequence WNL phase. The dotted lines give isochrones for 1, 2, and 3 Myr. On the basis of this comparison, one finds a cluster age of R136a of ~ 2 Myr.

isochrone. This number is in agreement with the age derived by KHH for the Wolf-Rayet–like stars R136a1 and R136a3 and Melnick 42.[14] As pointed out in § 3.3, we cannot exclude that the effective temperatures derived in this paper may be systematically underestimated owing to the neglect of line blanketing in our models. If the temperatures of O3-type stars are as high as ~ 50 kK as found by the Munich group (see, e.g., Kudritzki et al. 1992), a shift of ~ 0.05 dex should be applied to our derived values. This would imply that the highest mass stars in R136a formed only ~ 1 Myr ago (Massey & Hunter 1998).

Why is R136a so rich in stars of spectral type O3? Recall that Savage et al. (1983) considered it so unlikely that R136a could contain dozens of stars of such a very rare spectral type that they resorted to the hypothesis that R136a was dominated by the presence of a single or a few supermassive stars. The question may be rephrased as why do all the brightest cluster members fall in a small range in T_{eff}, with values typical for O3 stars? This can be understood by looking at the behavior of the theoretical isochrones: *The derived T_{eff} values are so similar because the isochrone for ~ 2 Myr runs almost vertical and because the distance in temperature between the isochrones of 1 and 3 Myr is very small.*

The effective temperatures of the program stars have been derived assuming a metallicity $Z = 0.004$ for R136a. Suppose we would have adopted $Z = 0.008$. How would this have affected the derived cluster age? There are two effects that need to be considered: (1) as pointed out in § 3.3, an increase in metallicity by a factor of 2 would lead to a decrease in derived temperatures by typically ~ 1500–1800 K; and (2) for $Z = 0.008$, the ZAMS, as well as the isochrones of the first few million years, shift toward lower temperatures compared to the $Z = 0.004$ tracks. The extent of this shift is ~ 1000–1500 K (Meynet et al. 1994). As both effects work in the same direction, only a slightly lower age—by some 200,000 yr—is derived for R136a in case of a metallicity $Z = 0.008$.

In addition to the presented empirical isochrone, it will be obvious that observed surface abundances also represent important constraints on models of the evolution of very massive stars. We have discussed the oxygen abundance in § 4.1 and have pointed out that only the brightest star in our sample, R136a5, displays a significant oxygen depletion. The brightest but one, R136a7, does not appear to show processed oxygen at its surface. This allows us to present the following, additional constraint: Incorporating the observed mass loss in evolution calculations, one expects that oxygen depletion should first occur at an age of 2–2.5 Myr in a star with an initial mass somewhere in the range from ~ 60 to 75 $M_\odot$. Although a detailed abundance analysis of the brightest members of R136a has not been the main focus of this paper, it is clear that this should have high priority in future quantitative studies of this cluster.

7.2. Stellar Mass and Mass Loss

A comparison of the stellar positions in the H-R diagram with the Meynet et al. tracks for $Z = 0.004$ yield current masses that differ only marginally from their expected initial masses. The reasons are obviously the very low mass

loss—e.g., the stars at $\log (L/L_\odot) \lesssim 5.5$ start their lives with a $\dot{M} \sim 2 \times 10^{-7}$ $M_\odot$ yr^{-1}—and the young age of ~ 2 Myr. The mass-loss rates used in the tracks imply that even the most luminous star R135a5, positioned on the track for $M_i = 76$ $M_\odot$, has not lost more than 3 $M_\odot$. All initial masses determined from a comparison with the $Z = 0.004$ Geneva tracks are given in the ninth column of Table 2.

For the stars with, say, $M_i \lesssim 50$ $M_\odot$, one does not expect that incorporation of the *observed* mass loss in track calculations leads to a much different current mass compared to that of Meynet et al. For instance, for star R136a-533, a time-integrated mass loss equal to the observed value will still amount to only a loss of some 3 $M_\odot$. However, for the most luminous stars, i.e., those corresponding to $M_i \gtrsim 50$ $M_\odot$, the current stellar masses implied by the observed mass loss may be substantially lower. For instance, again assuming a time-integrated mass loss equal to the observed value, one finds current masses of 30 and 35 $M_\odot$ for stars R136a5 and 608, respectively. The initial masses of these stars, as given in Table 2, are 76 and 57 $M_\odot$, respectively. Clearly, the given current masses are likely lower limits as observed $\dot{M}(L, T_{eff})$ relations point to an increase of mass loss with increasing main-sequence age (see § 5.3). The intricate coupling between mass and mass loss in track calculations may become even more clear when one realizes the following: Adopting a higher observed mass loss in new evolutionary track calculations will result in a slower increase of the luminosity in the main-sequence phase. This implies that it is a track with a *higher initial mass* that reaches the same point in the H-R diagram as does an available lower mass loss track. Consequently, tracks using a customized mass loss will likely yield both higher initial and current evolutionary masses.

In any case, it is clear one may conclude that *for the brightest members ($M_i \gtrsim 50$ $M_\odot$) one may anticipate that new evolutionary tracks, incorporating the observed $\dot{M}$ rates, will yield qualitatively different results compared to current calculations of very massive star evolution.* For the least luminous stars in our sample ($M_i \sim 40$ $M_\odot$), differences are expected to be much less dramatic. One such a qualitatively different result has been pointed out by KHH. They showed that the R136a stars initially more massive than ~ 100 $M_\odot$ are experiencing a hydrogen-rich WNL-like phase while on the main sequence. Current evolution calculations do not predict such a phase. All these reasons show the need for customized evolutionary tracks for the very massive stars in R136a. We intend to calculate such tracks in the near future. Finally, such calculations, combined with evolution synthesis, may yield new insight in the stellar composition and formation history of starburst clusters—for which R136a is a prototype—and starburst galaxies.

---

[14] Note, however, that Melnick 42 is positioned somewhat outside of the cluster and may not have been formed at the same time.

REFERENCES

Abbott, D. C. 1982, ApJ, 259, 282
Allen, C. W. 1973, Astrophysical Quantities (3d ed.; London: Athlone)
Campbell, B., et al. 1992, AJ, 104, 1721
Castor, J. I., Abbott, D. C., & Klein, R. I. 1975, ApJ, 195, 157
Charbonnel, C., Meynet, G., Maeder, A., Schaller, G., & Schaerer, D. 1993, A&AS, 101, 415
Chlebowski, T., & Garmany, C. D. 1991, ApJ, 368, 241
Chlebowski, T., Harnden, F. R., Jr., & Sciortino, S. 1989, ApJ, 341, 427
Conti, P. S., & Burnichon, M. L. 1975, A&A, 38, 467
de Jager, C., Nieuwenhuijzen, H., & van der Hucht, K. A. 1988, A&AS, 72, 259
de Koter, A. 1997, in ASP Conf. Proc. 120, Luminous Blue Variables: Massive Stars in Transition, ed. A. Nota & H. J. G. L. M. Lamers (San Francisco: ASP), 66
de Koter, A., Heap, S. R., & Hubeny, I. 1997, ApJ, 477, 792 (KHH)
de Koter, A., Hubeny, I., Heap, S. R., & Lanz, T. 1994, ApJ, 435, L71
de Koter, A., Schmutz, W., & Lamers, H. J. G. L. M. 1993, A&A, 277, 561
Gabler, A., Gabler, R., Pauldrach, A. Puls, J., & Kudritzki, R.-P. 1990, in ASP Conf. Proc. 7, Properties of Hot Luminous Stars, ed. C. D. Garmany (San Francisco: ASP), 218
Garmany, C. D., & Conti, P. S. 1984, ApJ, 284, 705
Gayley, K. G., Owocki, S. P., & Cranmer, S. R. 1995, ApJ, 442, 296
Groenewegen, M. A. T., & Lamers, H. J. G. L. M. 1989, A&AS, 79, 359
Groenewegen, M. A. T., Lamers, H. J. G. L. M., & Pauldrach, A. W. A. 1989, A&A, 221, 78
Haser, S. M., Pauldrach, A. W. A., Lennon, D. J., Kudritzki, R.-P., Lennon, M., Puls, J., & Voels, S. A. 1998, A&A, 330, 285
Heap, S. R., Ebbets, D., Malumuth, E., de Koter, A., & Hubeny, I. 1998, in preparation
Heap, S. R., Ebbets, D., Malumuth, E., Maran, S. P., de Koter, A., & Hubeny, I. 1994, ApJ, 435, L39
Herrero, A. 1994, in Evolution of Massive Stars, ed. D. Vanbeveren, W. van Rensbergen, & C. de Loore (Dordrecht: Kluwer), 137
Herrero, A., Kudritzki, R.-P., Vilchez, J. M., Kunze, D., Butler, K., & Haser, S. 1992, A&A, 261, 209
Howarth, I., & Prinja, R. K. 1989, ApJS, 69, 527
Hubeny, I., & Lanz, T. 1995, ApJ, 439, 875
Kudritzki, R.-P. 1980, A&A, 85, 174
Kudritzki, R.-P., Hummer, D. G., Pauldrach, A. W. A., Puls, J., Najarro, F., & Imhoff, J. 1992, A&A, 257, 655
Kudritzki, R.-P., Lennon, D. J., & Puls, J. 1995, in Science with the Very Large Telescope, ed. J. R. Walsh & I. J. Danziger (Garching: ESO), 246
Kudritzki, R.-P., Palsa, R., Feldmeier, A., Puls, J., & Pauldrach, A. W. A. 1996, in Röntgenstrahlung from the Universe, ed. H. U. Zimmermann, J. Trümper, & H. Yorke (MPE Report 263) (Garching: MPE), 9
Kudritzki, R.-P., Pauldrach, A. W. A., & Puls, J. 1987, A&A, 173, 293
Kudritzki, R.-P., Pauldrach, A. W. A., Puls, J., & Abbott, D. C. 1989, A&A, 219, 205
Kurucz, R. L. 1988, IAU Trans., 20b, 168
Lamers, H. J. G. L. M., & Cassinelli, J. P. 1996, in ASP Conf. Proc. 98, From Stars to Galaxies: The Impact of Stellar Physics on Galactic Evolution, ed. C. Leitherer et al. (Dordrecht: Kluwer), 162
Lamers, H. J. G. L. M., Cerruti-Sola, M., & Perinotto, M. 1987, A&A, 314, 726
Lamers, H. J. G. L. M., & Leitherer, C. 1993, ApJ, 412, 771

Lamers, H. J. G. L. M., Snow, T. P., & Lindholm, D. M. 1995, ApJ, 455, 269
Leitherer, C. 1988, ApJ, 326, 356
Leitherer, C., Schmutz, W., Abbott, D.C., Hamann, W.-R., & Wessolowski, U. 1989, ApJ, 346, 919
Lucy, L. B. 1982, ApJ, 255, 286
Lucy, L. B., & Abbott, D. C. 1993, ApJ, 405, 738
Lucy, L. B., & Solomon, P. M. 1970, ApJ, 159, 879
Lucy, L. B., & White, R. L. 1980, ApJ, 241, 300
Malumuth, E. M., & Heap, S. R. 1994, AJ, 107, 1054
Massey, P., & Hunter, D. A. 1998, ApJ, 493, 180
Melnick, J. 1985, A&A, 153, 235
Meynet, G., Maeder, A., Schaller, G., Schaerer, D., & Charbonnel, C. 1994, A&AS, 103, 97
Owocki, S. P. 1994, in Instability and Variability of Hot Star Winds, ed. A. F. J. Moffat, A. W. Fullerton, S. P. Owocki, & N. St-Louis (Dordrecht: Kluwer), 3
Owocki, S. P., Castor, J. I., & Rybicki, G. B. 1988, ApJ, 335, 914
Panagia, N., Gilmozzi, R., Macchetto, F., Adorf, H.-M., & Kirshner, R. P. 1991, ApJ, 380, L23
Parker, J. W., Heap, S. R., & Malumuth, E. M. 1995, ApJ, 448, 705
Pauldrach, A. W. A. 1987, A&A, 183, 295
Pauldrach, A. W. A., Kudritzki, R.-P., Puls, J., & Butler, K. 1990, A&A, 228, 125
Pauldrach, A. W. A., Kudritzki, R.-P., Puls, J., Butler, K., & Hunsinger, J. 1994, A&A, 283, 525 (PKPBH)
Pauldrach, A. W. A., Puls, J., & Kudritzki, R.-P. 1986, A&A, 164, 86
Puls, J., et al. 1996, A&A, 305, 171 (P96)
Santolaya-Rey, A. E., Puls, J., & Herrero, A. 1997, A&A, 323, 488
Savage, B. D., Fitzpatrick, E. L., Cassinelli, J. P., & Ebbets, D. C. 1983, ApJ, 273, 597
Savage, B. D., & Mathis, J. S. 1979, ARA&A, 17, 73
Schaerer, D., Meynet, G., Maeder, A., & Schaller, G. 1993, A&AS, 98, 523
Schaerer, D., & Schmutz, W. 1994, A&A, 288, 231
Schaller, G., Schaerer, D., Meynet, G., & Maeder, A. 1992, A&AS, 96, 269
Schmutz, W. 1991, in Stellar Atmospheres: Beyond Classical Models, ed. L. Crivellari, I. Hubeny, & D. G. Hummer (NATO ASI Series C, Vol. 341) (Dordrecht: Kluwer), 191
Schmutz, W., Hamann, W.-R., & Wessolowski, U. 1989, A&A, 210, 236
Sellmaier, F., Puls, J., Kudritzki, R.-P., Gabler, A., Gabler, R., & Voels, S. A. 1993, A&A, 273, 533
Simon, K. P., Jonas, G., Kudritzki, R.-P., & Rahe, J. 1983, 125, 34
Springmann, U. 1994, A&A, 289, 505
Taresch, G., et al. 1997, A&A, 321, 531
Voels, S. A., Bohannan, B., Abbott, D. C., & Hummer, D. G. 1989, ApJ, 340, 1073
Walborn, N. R., Ebbets, D. C., Parker, J. W., Nichols-Bohlin, J., & White, R. L. 1992, ApJ, L13
Walborn, N. R., Lennon, D. J., Haser, S. M., Kudritzki, R.-P., & Voels, S. 1995, PASP, 107, 104
Walborn, N. R., & Nichols-Bohlin, J. 1987, PASP, 99, 40
Walborn, N. R., Nichols-Bohlin, J., & Panek, R. J. 1985, International Ultraviolet Explorer Atlas of O-Type Spectra from 1200 to 1900 Å (NASA RP 1155) (Washington, DC: NASA)